University of Stavanger

Faculty of Science and Technology

MASTER'S THESIS

Study program/ Specialization: M.Sc. Petroleum Engineering/ Reservoir Engineering	Spring semester, 2015 Restricted access
Writer: Patrycja Szczesiul	…… (Writer's signature)

Faculty supervisor: prof. Jann Rune Ursin, University of Stavanger

External supervisors: Jan Kåre Risbakk, PGNiG Upstream International AS
Zbigniew Król, PGNiG Upstream International AS

Thesis title:

Use of successive pressure build-up test data from well A-1 H in the Snadd field to obtain dynamic reservoir information

Credits (ECTS): 30

Key words: Pressure build-up testing Dynamic data analysis Snadd field Well A-1 H	Pages: 47 + enclosure: Appendix A (12) Stavanger, 07/07/2015 Date/year

University of Stavanger in cooperation with PGNIG Upstream International AS

Use of Successive Pressure Build-up Test Data from Well A-1 H in the Snadd Field to Obtain Dynamic Reservoir Information

by

Patrycja Szczesiul

Faculty of Science and Technology
University of Stavanger
July, 2015

Abstract

Well A-1 H in the Snadd field was put on test production at the beginning of 2013. Since then, a series of pressure build-up tests has been conducted. These aimed to allow the evaluation of the quality of the Lysing prospect and the viability of future production from the field.

In this study, the pressure response from nine pressure build-up tests throughout the period of ca two years is examined. These were conducted staring in February 2013, and lasted until October 2014. The analysis, run with Saphir software, reveals information about dynamic reservoir parameters, such as permeability, permeability thickness, skin and turbulence factor. The tests show good repeatability, as the pressure derivative overlay can be observed. The value of permeability thickness from tests oscillates around 3300 md.ft, whereas the value from the last test is considered to be the most reliable, 3620 md.ft.

From the analysis of the extended test – PBU-9, a clear boundaries' response was detected. Discussions lead to conclusion that this might be the aquifer response, the distance to the aquifer was estimated to be 4800 ft.

The change of the average reservoir pressure, p* with time was determined and it creates a reasonable trend for production from the field. In further studies the obtained pressure values can be a foundation for material balance calculations.

Acknowledgements

I take this opportunity to express my sincere gratitude to Mr Zbigniew Król from PGNIG Upstream International AS, who was of a great help to me, sharing his expertise and guiding me through the process of my work.

Also, thanks to the University of Stavanger for facilitating my studies, providing me with the necessary software and the place to work.

Finally, special thanks to my family and friends for their encouragement and support during writing this thesis.

Table of contents

List of figures

List of tables

Chapter 1 Introduction

The Snadd field, on the Norwegian Continental Shelf, is a relatively new gas field discovered in 2000 with well 6507/5-3. Until today, there have been several wells drilled in the field, out of which one – 6507/5-A-1 H – is still on stream. Since 2013 a series of test productions has been conducted in this well, in order to acquire reservoir information. The analysis of pressure transient tests would allow evaluating the quality of the prospect and the viability of future production. It would also be a foundation for material balance calculations and estimates of possible water encroachment into the well in the course of production.

1.1. Objectives and Scope of Work

The following report will present a way to obtain dynamic reservoir information of the Snadd prospect through a thorough analysis of nine pressure buildup tests performed on the test production well 6507/5-A-1 H, called later well A-1 H, over a period of about two years. With the use of Saphir software, the information about reservoir connectivity, permeability thickness product, permeability, skin values and turbulence factor will be obtained. The author will also determine a change in reservoir pressure with time, and will discuss how this information could be used in reservoir simulators to improve reliability and accuracy of the simulated results during history matching. The analysis of the last of the nine tests (PBU 9) will be used to evaluate if the existing data can support the presence of an aquifer. The distance from the well to this aquifer will be assessed and the implication of this knowledge will be discussed.

1.2. Literature Study

Literature review conducted as a part of this work falls into two categories:

- Documentation introducing information about the Snadd discovery and well A-1 H specific information;
- Papers and books addressing the studies carried out in the topic of pressure transient testing with emphasis on pressure buildup testing.

The first group of papers serves as a basis for understanding the Snadd field structure. The author briefly introduces conducted studies, providing information about geology, formation characteristics and depositional model of the field. Especially, the attention was paid to reports by BP from 2010 [1], 2013 [2] and 2014 [3], which contain thorough geological analyses together with seismic data and introduce the studies on the possible aquifer supporting the field. Relevant parameters describing the reservoir, used later as input data for simulations, were briefly presented. The author found it also relevant to include some basic information about the well, on which the tests were conducted. Documentation by BP from year 2011 [4] serves as basic source of information in that subject.

The other group of studied literature addresses the topic of pressure build-up analysis. The literature studied in that subject allowed understanding the development of the methods and the progress that can be observed in today's interpretation techniques.

Pressure build-up analysis methods date back to 1936 when Muskat [5] presented research indicating dependency between the slope of the latter part of the pressure curve and the value of the formation permeability. However, the first methods to identify and quantify IARF (infinite acting radial flow) were developed in 1950's. They were based on straight-line interpretation.

For instance, Miller, Dyes and Hutchinson [6] in their study from 1950 described the way to obtain the effective formation permeability, the average permeability and the average formation pressure from the build-up characteristics plotted with dimensionless variables of pressure and time in a Δp_D versus $\log(t_D)$ scale. In 1951 Horner [7] presented a method of obtaining permeability thickness product and average reservoir pressure, based on plotting the bottom hole shut-in pressure against the logarithm of $(t_p + \Delta t)/\Delta t$. On such created plot for the IARF part the pressure points fall on a straight line and the average reservoir pressure may be obtained through the means of extrapolation. Also, the parameters as permeability thickness and skin can be estimated from the behavior of the line's slope.
The overview of early analysis techniques can be found in the paper by Perrine [8], where the similarities and differences between different approaches have been pointed out.

In 1970's the log-log type-curve matching techniques were implemented. Ramey [9] introduced the method which utilized curves, which are a set of preplotted solutions to the flow equations for certain type of formations, with altering initial and boundary conditions. The solutions are plotted with dimensionless variables in a log-log scale [10]. The idea behind type-curve matching is to compare real data plotted on log-log scale with the theoretical response (pre-printed type-curves). This allows choosing the best model match, providing the interpreter with physical results. The early study conducted in the area of type-curve matching is summarized in a paper by Earlougher and Kersch [11]. Gringarten et al. [12] introduced type-curves plotted in p_D versus t_D/C_D scale, where each plot depends on parameter C_De^{2s}. The shape of the pressure response is different for different values of C_De^{2s}. The method became widely used, however, for great values of C_De^{2s} the shapes of the curves are very similar and obtaining the model-specific solution becomes doubtful.

In 1983, Bourdet et al. [13] introduced a new generation of pressure-derivative type-curves. The technique assumes plotting the pressure difference Δp and its derivative against time in a log-log scale. The Bourdet derivative is a slope of the semi-log plot displayed in a log-log scale. This technique significantly decreased the possibility of improper match as pressure derivative curves exhibit distinctly different trace for different values of C_De^{2s}.

Starting from mid-1980's more and more advanced methods were introduced, utilizing computer software and implementing numerical models into simulations. The Bourdet derivative, however, has remained the core diagnostic tool until today. Software became powerful tool for analysis, allowing considering all the production period from the well and taking advantage of nonlinear regression. The tedious calculations turned into quick parameter change in a dialog window. The results are more accurate and are based on pre-defined set of equations, almost for each case of well and reservoir behavior that can be encountered in practice.

The report is organized as follows:

- Chapter two introduces a brief description of Snadd field and well A-1 H. In particular, the structure of the field and the values of specific parameters used as input data for further modeling are introduced.
- Chapter three covers the theoretical basis for pressure build-up analysis. The adequate workflow are described, including basic assumptions and relevant models.
- Chapter four contains the experimental part of the work. The analysis, including simulations for the considered tests is presented.
- Chapter five is devoted to discussions and results' comparison.
- Chapter six is a conclusion of the report

Chapter 2 Snadd Field and Well A-1 H Information

2.1. Snadd Field Overview

The Snadd field is located in the Norwegian Sea, about 210 km off the coast from Sandnessjøen, Norway. It consists of Snadd South, Snadd North and Snadd Outer. Being between 2 and 3 km wide and even up to 56 km long, the field might be one of the Norway's longest gas fields discovered so far [2]. Snadd is located within the Skarv unit area (blocks 6507/2, 6507/3 and 6507/5) between Norne oil field in the North, and Heidrun gas field in the South.

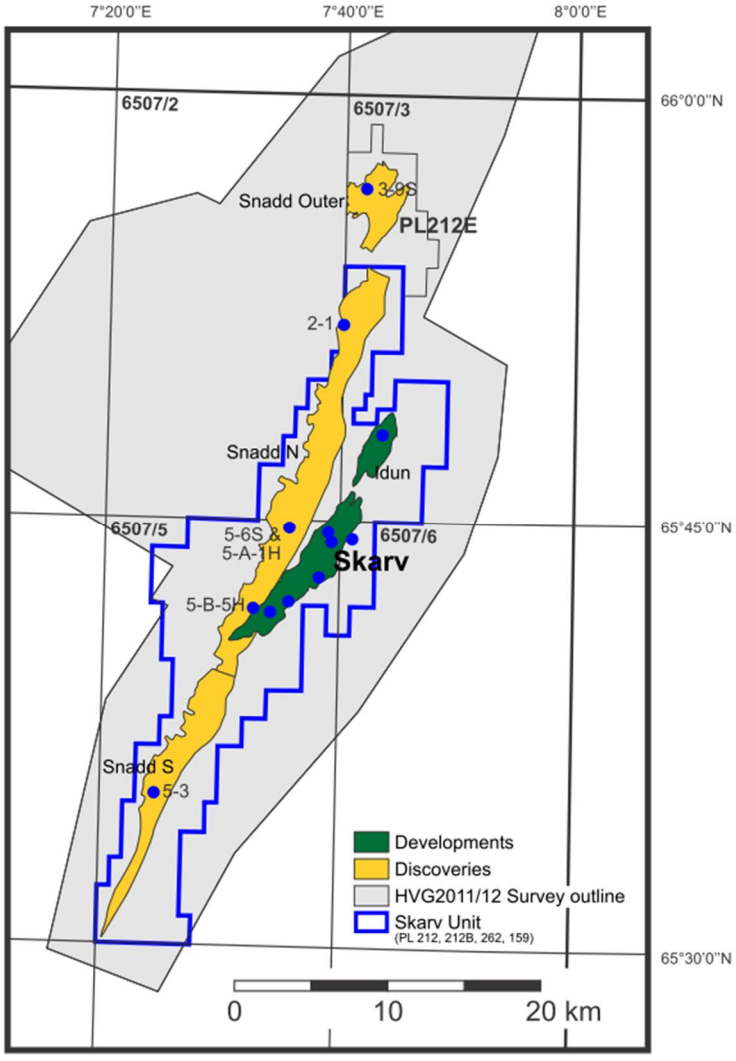

Figure 2-1: Snadd field outline [1]

2.1.1. Geological Setting and Depositional Model

The Snadd reservoir lies on a narrow, fault-bounded terrace that is a part of the Dønna Terrace, between the Trøndelag Platform to the East and the Rås Basin to the West [14]. The structure is relatively flat with a structural dip in the order of 2-3 degrees, dipping down towards thicker sands in the Rås basin [15].

The prospect is created by late Cretaceous sands of Turonian-early Coniacain age represented by Lysing and Lange formations. It consists of a heterogeneous succession of deep marine turbidite sandstones inter-bedded with minor mudstones [1].

In the inspected area, the reservoir lies at depths of about 2767 – 2799 m TVDSS (true vertical depth mean sea level), with sea depths of 350-370 m. The trap hosting the Snadd discovery is a combined structural and stratigraphic trap with three way closure [15]. It is defined by seismic; to the west the trap is structural and is formed by simple dip. To the east the trap is defined by a combination of stratigraphic pinch-out and faulting [1].

2.1.2. Log Interpretation and Petrophysics

Well log data together with information acquired from the core analyses and seismic data give an outline of petrophysical properties of the Snadd prospect. In particular, information about porosity, water saturation and reservoir temperature has been obtained.

Net to gross ratio

Based on the VSH (volume of shale) calculations from gamma ray and neutron-density logs, the net to gross (N/G) ratio for the Lysing reservoir was determined to be 0.88 [1].

Pore system and porosity estimate

The porosity of the reservoir rock was calculated from neutron-density logs. Total porosity (PHIT) was determined at the level of 0.25 and the effective porosity (PHIE) at the level of 0.21 [16].

Temperature

Temperature measurements oscillate around 95 deg C, which is consistent with a regional temperature trend for Lysing formation [1]. The reservoir temperature used in simulations has a value of 100 deg C (212 deg F). The reservoir temperature is not expected to exceed this value [15].

Water saturation

The analyses indicate that the Snadd North prospect is of high water saturation and relative low permeability. Water saturation was calculated to be 0.4 [16].

Formation compressibility of the reservoir rock was determined at $c = 3.43 \cdot 10^{-6}\, 1/PSI$

2.1.3. Prospect Pressure and Fluids

Based on PVT analysis of fluid samples, gas specific gravity and formation volume factor were calculated to be 0.673 and $3.47 \cdot 10^{-3}\ m^3/Sm^3$, respectively [17]. A gas-water contact for well A-1 H is estimated at 2828 m TVDSS [1]. The initial reservoir pressure p_i for the Lysing reservoir in the area is 5362 psia [16]. Snadd North gas samples indicate 0.5 mole% content of CO2 [2].

2.1.4. Summary

The summary of the main parameters and properties of the Snadd North prospect, based on well A-1 H, are presented in table 2.1.

Table 2-1: Snadd reservoir properties, based on well A-1 H

Parameter	Symbol	Value	Unit
Top Lysing		2767	m TVDSS
Base Lysing		2799	m TVDSS
Thickness	h	32	m
Net to gross ratio	N/G	0.88	-
Gas-water contact	GWC	2834	m TVDSS
Formation compressibility	c	3.43E-06	1/psi
Total porosity	PHIT	0.25	-
Effective porosity	PHIE	0.21	-
Water saturation	S_w	0.4	-
Formation volume factor	Bg	3.47E-03	m^3/Sm^3
Gas specific gravity	GSG	0.673	-
CO2 content		0.5	mole %
Reservoir temperature	T	95.4	deg C
Initial reservoir pressure	p_i	5362	psia

2.2. Well A-1 H Information

Well A-1 H is a test producer located near the middle of the Snadd North structure. It was put on long term test in 2013 to evaluate the main dynamic uncertainties associated with the Lysing formation. As can be seen in Figure 2-2, the well is highly deviated within the Lysing structure.

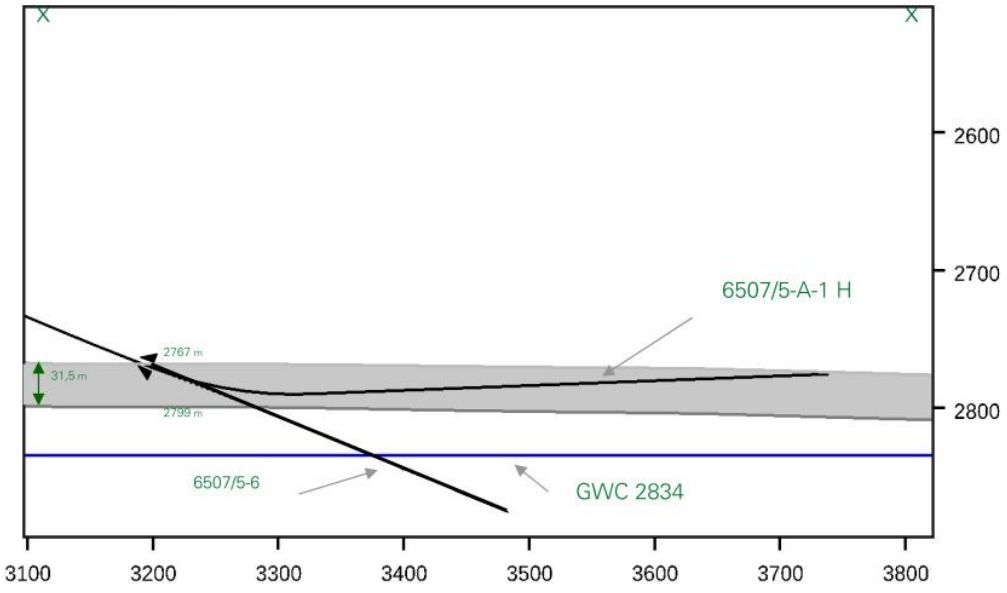

Figure 2-2: Cross-section along Snadd producer [18]

Figure 2-3 illustrates a map showing the well location relative to the interpreted Lysing sand pinch-out and gas water contact.

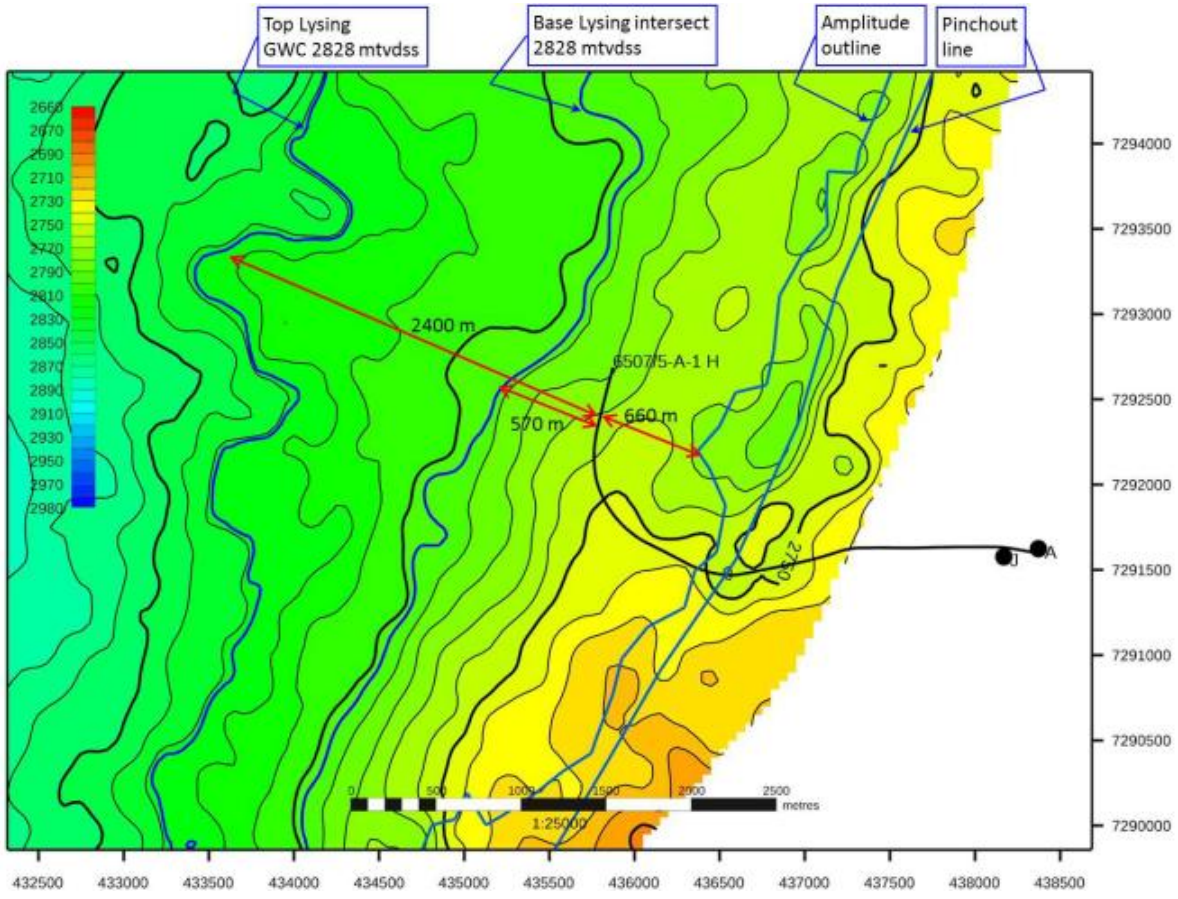

Figure 2-3: Well A-1 H location relative to Lysing pinch-out [3]

Well A-1 H was drilled from the Skarv A template as a sidetrack from the Snadd North exploration well 5-6 ST2 in 2011, kicked off below the already installed 9 7/8'' casing. The well is completed as a horizontal producer, with 5 ½'' wire-wrapped screens and successfully gravel packed [4].

The main objective to drill a production sidetrack was to perform long term production testing on Snadd North. The results would help resolve the main uncertainties for long term well productivity on Snadd, i.e. water influx and stratigraphic compartmentalization [18].

Chapter 3 Pressure Build-up Tests Theory

3.1. Introduction

In the introduction of the report, the highlights of the pressure build-up testing methods were outlined and the development of the techniques throughout the years has been briefly presented. The aim of this chapter is to deliver more specific information on the subject with focus on testing horizontal gas wells, as in the case of the well A-1 H. The methodology, basic assumptions and amount of information that can be extracted from a single analysis will be introduced.

As summed up by Ahmed in [19], studies in the field of well testing have proven that the pressure behavior of the reservoir caused by a rate change directly reflects geometry and flow properties of the reservoir. The typical build-up procedure looks as follows [20]:

1. Before a test: the well must have been flowing long enough to reach stabilized rate;
2. Once the stabilization is reached, the well is shut-in;
3. The increasing bottom hole pressure is observed (pressure response);
4. During shut-in period the flow rate must be controlled at the level of zero.

The plot of pressure versus logarithm of time obtained from a test shows a stretched-out S-line. The pressure points of the latter part of this curve create often nearly a straight line [8]. This line is the main part of interest for the interpreting engineer and it represents the Infinite Acting Radial Flow – IARF. IARF can be observed after well effects have subsided and before the reservoir boundaries are reached [21]. From the analysis of this curve, it is possible to determine parameters describing both reservoir and well, in particular, effective reservoir permeability, extent of formation damage around the wellbore, flow barriers and fluid contacts, initial and average reservoir pressure, drainage pore volume, communication between wells and also well production potential and well geometry [19, 20].

Units and conversion parameters

Further considerations will be presented in SI- and oil field units system – two most common unit systems used in well testing. Table 3-1 has been put together, based on Zolotukhin and Ursin [22], to keep the clarity of the presented workflow.

Table 3-1: System of units used in well test analysis
(modified from Ursin and Zolotukhin [22])

Parameter	Nomenclature	SI-units	Field units
Flow rate	q	Sm^3/d	STB/d
Volume factor	B	Rm^3/Sm^3	RB/STB
Thickness	h	m	ft
Permeability	k	μm^2	md
Viscosity	μ	mPa·s	cp
Pressure	p	kPa	psia
Radial distance	r	m	ft
Compressibility	c	$(kPa)^{-1}$	psi^{-1}
Time	t	hrs	hrs

1 STB/d = 0.159 Sm^3/d
1 ft = 0.3048 m
1 mD = $0.987 \cdot 10^{-3}$ μm^2
1 cp = 1 mPa·s
1 psi = 6.895 kPa

3.2. Basic Assumptions

The analysis of the well test responses is governed by relations resulting from the solution of the flow equations. In the following these will be briefly introduced.

Darcy's Law

The fundamental law used in well testing is Darcy's Law, established in 1856. It is a formulation of fluid flow in porous medium:

$$Q = A\frac{k}{\mu}\frac{\Delta p}{L} \tag{3-1}$$

The differential form of the equation reveals a relation between the flow rate across the surface and the pressure gradient across its section. It can be written in both linear and cylindrical coordinates for linear and radial flow. For linear flow it takes the form:

$$-\frac{\partial p}{\partial x} = \frac{q\mu}{kA} \tag{3-2}$$

For radial flow, if the assumption is made that the fluid flows across a cylindrical section of an isotropic medium and the flow rate is positive in direction of the well, it takes the form:

$$r\frac{\partial p}{\partial r} = \frac{q\mu}{2\pi kh} \tag{3-3}$$

In case of turbulence, Darcy's law is replaced by the Forcheimer's equation, which is used to describe the non-Darcy flow. This kind of problems are usually solved with numerical models [21].

Diffusivity Equation

As formulated by Houzé et al. in Dynamic Data Analysis [21] "the diffusivity equation describes how, in an elementary piece of rock, the pressure will react in time as a function of the local pressure gradient around that piece of rock". The equation is derived as a combination of the law of conservation of matter, Darcy's Law and an equation of state [23]. In its simplest form it can be written:

$$\frac{\partial p}{\partial t} = \frac{k}{\phi\mu c_t}\left[\frac{\partial}{\partial r}\left(\frac{\partial p}{\partial r}\right) + \frac{1}{r}\left(\frac{\partial p}{\partial r}\right)\right] \tag{3-4}$$

The equation might take different forms, based on pre-made assumptions. The basic set of assumptions for the equation formulated as above is:

- Homogeneous and isotropic reservoir;
- Single-phase fluid, slightly compressible;
- Darcy's law applies;
- Reservoir and fluid properties are independent of the pressure.

Solution for the Infinite Acting Radial Flow

The infinite acting radial flow – IARF is a main part of interest during the analysis of the pressure response. It occurs when fluid flows into the well equally from all the directions [24], until a boundary is reached. In vertical wells it may be observed when the wellbore is penetrating the formation, being placed perpendicular to its sealing boundaries. The regime can

be also observed in horizontal wells, when the flow lines converge in the direction of the well, when the flow stabilizes (see section 3.5).

Solving the diffusivity equation for the IARF is a foundation for well testing. In order to obtain this, the following boundary conditions are introduced (according to Schlumberger [24]):

- Initial boundary condition: for the most common case, it is assumed that the reference time is t=0 and the initial reservoir pressure is p_i. The pressure is identical everywhere in the reservoir. The initial boundary condition is:

$$p_{t=0\rightarrow r} = p_i \tag{3-5}$$

- Inner boundary condition: the condition of constant volumetric rate at the sandface; in Darcy units:

$$\left[r\frac{\partial p}{\partial r} \right]_{r_w} = \frac{q_{sf}\mu}{2\pi kh} \tag{3-6}$$

- Source well: the assumption of the infinitesimal well radius:

$$\lim \left[r\frac{\partial p}{\partial r} \right]_{r\rightarrow 0,t} = \frac{qB\mu}{2\pi kh} \tag{3-7}$$

- Outer boundary condition: assumption of the reservoir of infinite extent:

$$\lim_{r\rightarrow\infty} \left[p(r,t) \right] = p_i \tag{3-8}$$

Dimensionless variables

For the needs of the analysis, the above equations are expressed in terms of dimensionless variables. The following relations, in oil field units, are incorporated [24]:

Dimensionless distance:

$$r_D = \frac{r}{r_w} \tag{3-9}$$

Dimensionless time:

$$t_D = 0.000264\frac{kt}{\phi\mu c_t r_w^2} \tag{3-10}$$

Dimensionless pressure:

$$p_D = \frac{1}{141.2}\frac{kh}{qB\mu}(p_i - p) \tag{3-11}$$

The equations 3-4 to 3-8 expressed in dimensionless variables become [24]:

Diffusivity:

$$\frac{\partial p_D}{\partial t_D} = \frac{1}{r_D}\frac{\partial}{\partial r_D}\left(r_D \frac{\partial p_D}{\partial t_D}\right) \tag{3-12}$$

Inner condition:

$$\lim\left[r_D \frac{\partial p_D}{\partial r_D}\right]_{r_D \to 0, t_D} = 1 \tag{3-13}$$

Initial condition:

$$p_{D_{tD=0,rD}} = 0 \tag{3-14}$$

Outer condition:

$$\lim_{r_D \to \infty}\left[p_D(r_D, t_D)\right] = 0 \tag{3-15}$$

And line source well solution (radial solution) for homogeneous reservoir of infinite extent:

$$p_D = -\frac{1}{2}E_i\left(-\frac{{r_D}^2}{4t_D}\right) \tag{3-16}$$

With the late-time approximation taking the form:

$$p_D = \frac{1}{2}\left[\ln(t_D) + 0.80907\right] \tag{3-17}$$

Equation 3-17, relating the pressure to the natural logarithm of the time, in radial flow is a fundamental equation for well test interpretation. For damaged and stimulated wells, the modification to the equation 3-17 is introduced [24]:

$$p_D = \frac{1}{2}\left[\ln(t_D) + 0.80907 + 2S\right] \tag{3-18}$$

3.3. Wellbore storage and skin

Wellbore storage:

Once the valve opening the well is opened at the surface, the flow from the well will begin. What is observed first, is a wellbore storage effect – the fluid produced at the beginning of the flow is not yet flowing from the reservoir, but it is a volume that was present in the wellbore. Similarly, once the valve is closed, the flow from the reservoir will continue until there is no

more space in the wellbore for the fluid to compress. In fact, the time the rate becomes zero at the sandface is with retardation to the time, the well is actually shut-in. This transition time is a time of wellbore storage. Figure 3-1 illustrates the wellbore storage implications on the flow rate for production start and well shut-in. As long as the wellbore storage affects the pressure response, no useful reservoir information can be obtained.

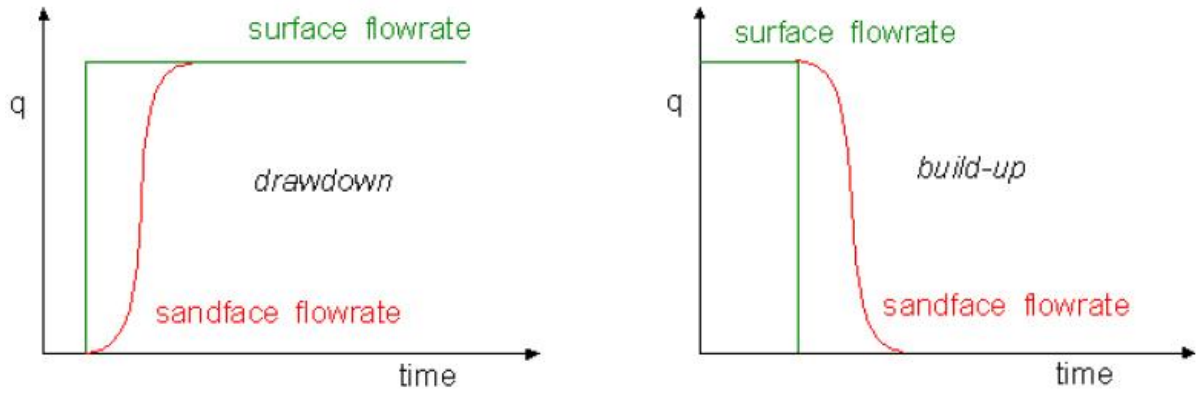

Figure 3-1: Wellbore storage effect [24]

Skin:

Skin a dimensionless factor representing the difference between the effective productivity of a well in an ideal case compared to the reality. Skin value equal to zero means the pressure drop in a completed and perforated wellbore is consistent with what would be expected based on ideal case. Positive skin indicates near-wellbore damage and thus a higher pressure drop. Negative skin implies smaller pressure drop near the wellbore, thus better productivity from the well. In figure 3-2, the scheme of the pressure drop for negative and positive skin may be observed.

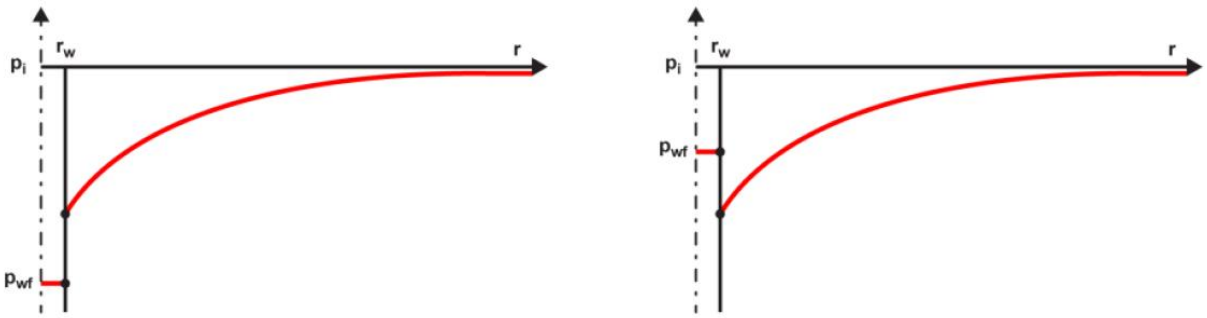

Figure 3-2: Skin sign convention [21], left S<0, right S>0

In the case of horizontal wells skin consists of geometrical skin S_G and mechanical skin S_0. S_{tot} combines these two providing the information about the total skin.

3.4. The analysis

Semi-log approach:

Semi-log approach is a classical method of interpretation for the needs of well testing. In radial flow, the pressure change depends on the logarithm of time, that means, once the pressure is plotted versus the log of time, the IARF will show a straight line. The parameters obtained from that straight line are permeability thickness product and skin, the slope m can be calculated as follows [24]:

The equation 3-18, expressed in decimal logarithms takes the form:

$$p_D = 1.151\log(t_D) + 0.40453 + S \tag{3-19}$$

In terms of real pressure, in field units, it can be rewritten as:

$$\Delta p = 162.6\frac{q\mu B}{kh}\left[\log(\Delta t) + \log\left(\frac{k}{\phi\mu c_t r_w^2}\right) - 3.23 + 0.87S\right] \tag{3-20}$$

The slope m of the straight line in Δp, or p versus log(Δt) scale is then:

$$m = 162.6\frac{q\mu B}{kh} \tag{3-21}$$

The value of permeability thickness product kh may be obtained from straight line slope, assuming the q, μ and B parameters are known. Skin is obtained from the relation:

$$\frac{\Delta p_{1h}}{m} = \left[\log\left(\frac{k}{\phi\mu c_t r_w^2}\right) - 3.23 + 0.87S\right] \tag{3-22}$$

One of the most popular semi-log plots, plotted in p versus log(Δt) scale is the Miller-Dyes-Hutchinson (MDH) plot. However, this is valid only for the first drawdown test on the well.

To be extended to build-up response use, the method introduced by Horner [7] has to be implemented [24]. In the method the solution for IARF in the build-up case looks as follows:

$$p = p_i - 162.6\frac{q\mu B}{kh}\log\left(\frac{t_p + \Delta t}{\Delta t}\right) \tag{3-23}$$

Equation 3-23 reveals the linearity between the pressure drop and Horner time function $\log(\frac{t_p+\Delta t}{\Delta t})$. The slope line for this solution is also expressed by equation 3-21. The skin for this solution can be defined as:

$$S = 1.151\left[\frac{\Delta p_{1h}}{m} - \log\left(\frac{k}{\phi\mu c_t r_w^2}\right) + \log\left(\frac{t_p + 1}{t_p}\right) + 3.23\right] \tag{3-24}$$

The scheme of a Horner plot is illustrated in figure 3-3.

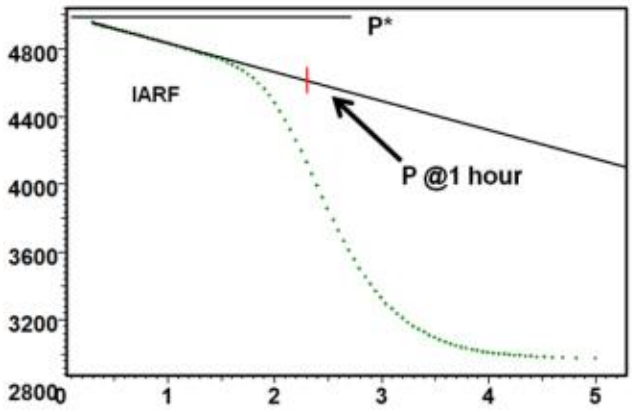

Figure 3-3: Horner plot [21]

Superposition time function:

Superposition time function is a general semi-log plot used for interpretations, it applies to all transients [24]. It is expressed as:

$$Sn(\Delta t) = \sum_{i=1}^{n-1}(q_i - q_{i-1})\log\left[\sum_{j=1}^{n-1}\Delta t_j + \Delta t\right] + (q_{ni} - q_{n1})\log(\Delta t) \tag{3-25}$$

In the superposition time the x-axis is in Cartesian scale – superposition time function is itself logarithmic with, with all the time values in the expression being log terms [24]. The slope of the IARF straight line becomes m', where m'=m/q and q is q(Δq) which is a change in rate of transient; in case of build-up tests, the flow prior to shut-in.

Log-log approach:

Schlumberger [24] in Introduction to Well Testing present the log-log analysis approach the following way:

The log-log approach is based on dimensionless variables of pressure and time p_D and t_D. Working on pressure and time in dimensionless variables, the analytical model of the well and reservoir with typical responses can be created, or the type-curve providing with a global description of the pressure response, which is independent of flow-rate or the actual values of the reservoir parameters.

When the proper dimensionless model is selected the real (log Δp vs log Δt) and theoretical (log p_D vs log t_D) pressure curves are of the same shape. Once the model is identified, parameters as wellbore storage (c), permeability thickness product (kh) and skin can be extracted [24].

3.5. Pressure derivative

The pressure derivative method introduced by Bourdet [13] is a powerful tool used in modern analysis. The pressure derivative is a slope of the semi-log plot plotted in a log-log scale. As formulated by Schlumberger [24], "the pressure derivative is essentially the rate of change of pressure with respect to the superposition time function". The idea behind the derivative is to calculate the slope at each point of the pressure curve on the semi-log plot and display it on a log-log plot.

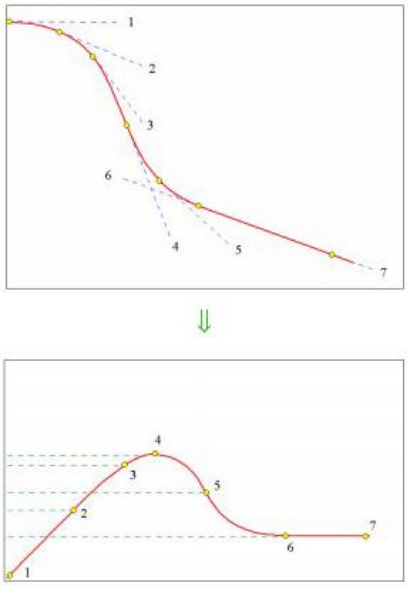

Figure 3-4: Pressure derivative schematic [24]

With the use of the natural logarithm, the derivative can be expressed as the time derivative, multiplied by the elapsed time Δt from the start of the production period, equation 3-26 [20]:

$$\Delta p' = \frac{dp}{d \ln \Delta t} = \Delta t \frac{dp}{dt} \tag{3-26}$$

Well with wellbore storage and skin in a homogeneous reservoir

Considerations about the analysis of the case of well with wellbore storage and skin in a homogeneous reservoir follow the interpretation path presented by Bourdet in Ref [20].

Radial flow: Once the radial flow to the wellbore is established, the derivative becomes constant. In the regime the characteristic log-log shape on the pressure curve will not be observed but it can be identified with the use of the pressure derivative.

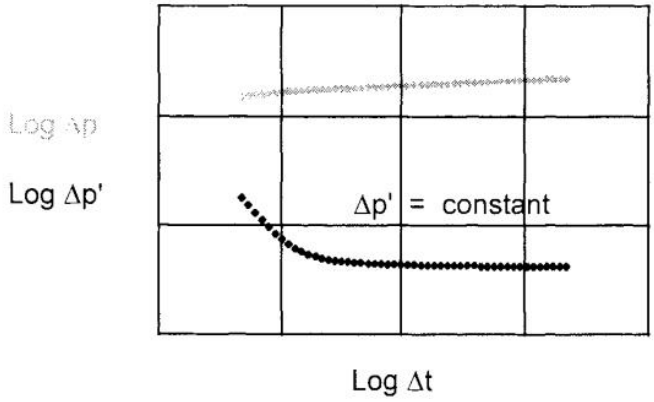

Figure 3-5: Pressure and derivative responses on log-log scale, radial flow [20]

Figure 3-5 illustrates the pressure and derivative responses on log-log scale, the value of Δp' is obtained from:

$$\Delta p' = 70.6 \frac{qB\mu}{kh} \tag{3-27}$$

In dimensionless variables, the derivative stabilizes at 0.5

$$p'_D = \frac{dp_D}{d \ln(t_D / c_D)} = 0.5 \tag{3-28}$$

Wellbore storage:

During the wellbore storage regime, the pressure change and the pressure derivative are identical. On log-log scales, the pressure and derivative curves merge following a straight line of slope equal to unity [20], figure 3-6.

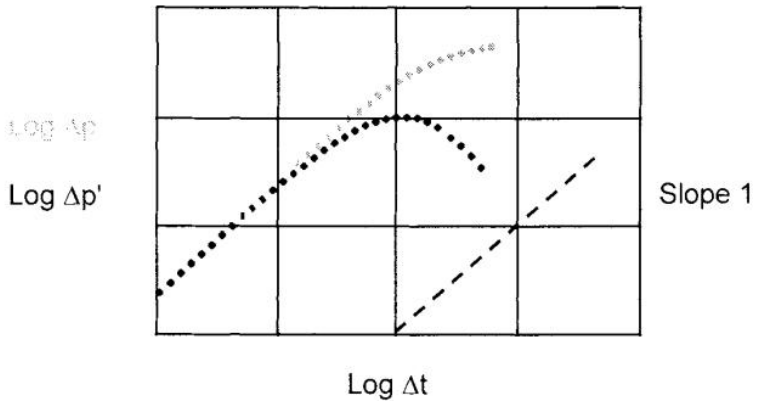

Figure 3-6: Pressure and derivative responses on log-log scale, wellbore storage [20]

Derivative interpretation essentials:

While for some cases, a clear response of the pressure behavior cannot be seen, the derivative will always display a characteristic response, allowing the further interpretation.

- For early time pressure and pressure derivative curves will merge on a unit slope straight line
- For radial flow regime the derivative stabilizes at a constant value, corresponding to the superposition slope m' [24].

3.6. Horizontal well case

Figure 3-1 illustrates a scheme of a horizontal well. In the following, it is assumed that the well produces from strictly horizontal reservoir of a uniform thickness h, with sealing upper and lower boundaries. The penetration length is 2L and z_w is a distance between the drain hole and the bottom sealing boundary; k_v and k_H stand for vertical and horizontal permeability, respectively.

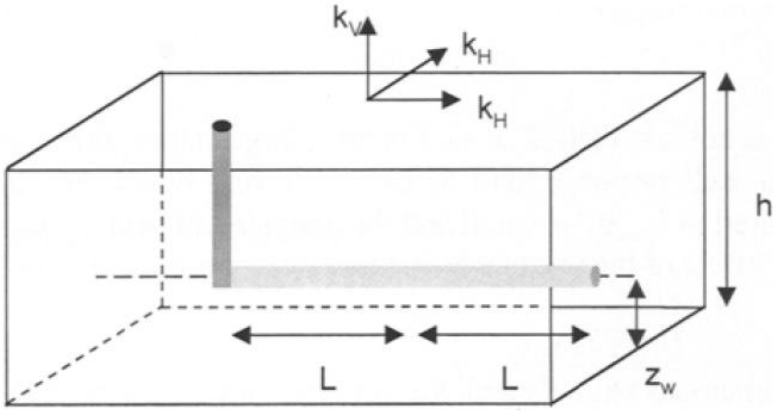

Figure 3-7: Horizontal well geometry [20]

During production from a horizontal well in an infinite system, three main flow regimes can be distinguished after wellbore storage effects have faded. These are [20, 24]:

1. **Early-time pseudo-radial flow**

   The first flow regime is a pseudo-radial flow, analogous to radial flow in a vertical well. The permeability thickness product is a combination of vertical and horizontal component (thickness corresponds to the producing well length). It is defined as:

   $$(kh)_{early} = 2L\sqrt{k_v k_H} \tag{3-29}$$

2. **Intermediate-time linear flow**

   Intermediate-time linear flow is the second flow regime observed when upper and lower boundaries are reached. In this case, the derivative follows a half-unit slope log-log straight line; *kh* takes the form:

   $$(kh)_{linear} = k_H L^2 \tag{3-30}$$

3. **Late-time radial flow**

   The flow regime observed when the flow lines converge from all reservoir directions towards the well; the flow analogous to the flow in a vertical well. The stabilization of the derivative corresponds to the infinite acting radial flow in the reservoir. The permeability thickness can be found from the relation:

   $$(kh)_{late} = k_H h \tag{3-31}$$

Figure 3-2 illustrates the schematic of the flow regimes for each case together with the direction of the flow lines. The corresponding pressure and derivative response can be observed in figure 3-3.

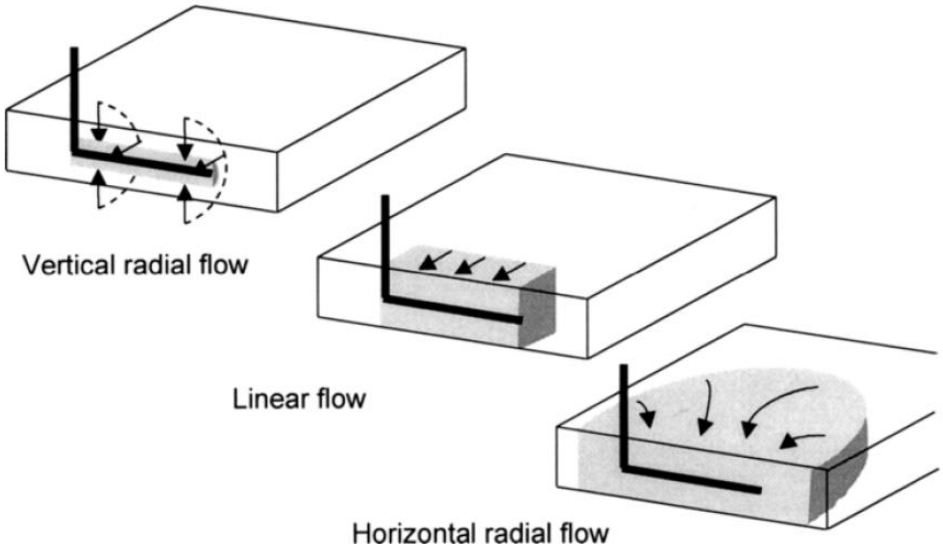

Figure 3-8: Horizontal well main flow regimes [20]

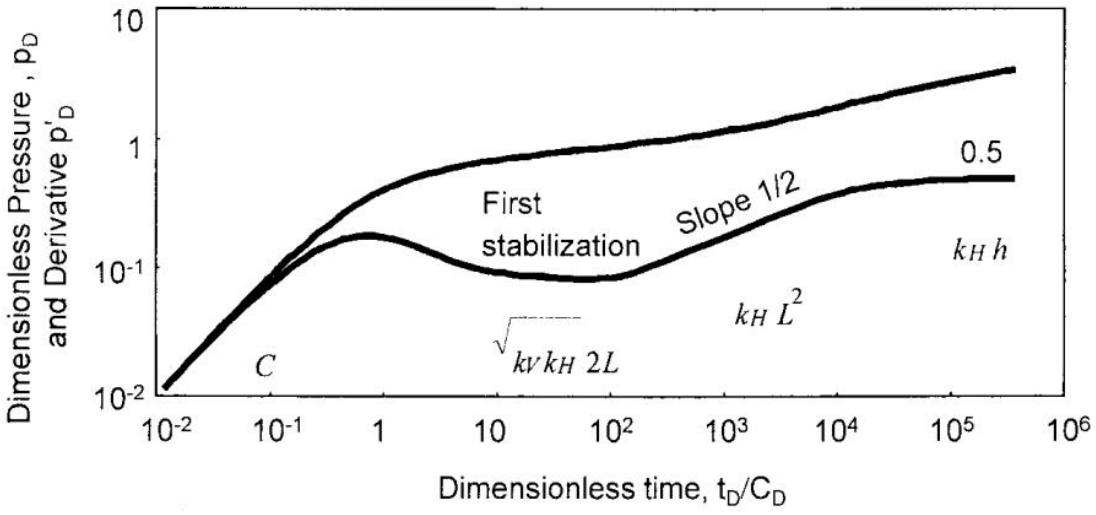

Figure 3-9: Horizontal well log-log response [20]

As summarized by Bourdet in [20] there have been several methods since mid-1980's which attempted presenting solution for horizontal wells. The solutions are approximate. They are based on a line source solution which can be applied only if the following condition is met: $t_D > r_{we}^2$. For large skin values, the condition at early time is not satisfied. Additionally, for a case when anisotropy between vertical and horizontal permeability is large the solutions reveal small discrepancies.

Bourdet [20] in his work from 2002 presented the equations governing horizontal flow regimes. Each of the regimes can be described with the unique pressure and dynamic reservoir parameters relationship. Additionally, the skin values for each flow were defined, including the pseudo-skin components.

3.7. Gas wells solution

For gas well tests analysis, the equation 3-4 has to be reformulated, because of the difference in phase behavior (compressibility of gas). Introducing the equation of state for real gases, equation 3-32, and the pseudo-pressure term, as presented by equation 3-33, it is possible to reformulate the basic diffusivity equation for the gas case.

$$PV = nZRT \tag{3-32}$$

$$m(p) = \int_{p_0}^{p} \frac{2p}{\mu(p)z(p)} \tag{3-33}$$

The diffusivity equation for gas phase is expressed as:

$$\Delta m(p) = \frac{\phi \mu c_t}{k} \frac{\partial m(p)}{\partial t} \tag{3-34}$$

Equation 3-34 may be rewritten in coordinates for radial flow. For the homogeneous isotropic reservoir, using the field units, it look as follows [21]:

$$\frac{\partial p}{\partial t} = 0.0002637 \frac{k}{\phi \mu c_t} \frac{1}{r} \left[\frac{\partial}{\partial r} \left(r \frac{\partial p}{\partial r} \right) \right] \tag{3-35}$$

Such formulated diffusivity equation is used in most analytical models for well test interpretation. It describes the flow of homogeneous reservoir, where everywhere in the reservoir the same equation applies. In case of modeling more complex reservoirs, the equation is replaced by other relevant formulations. [20]

Chapter 4 Snadd Field Dynamic Data Analysis

4.1. Data preparation

During the first stage of test production from well A-1 H, 9 BPUs have been performed. Some of these have taken advantage of facility shutdowns and some have been planned for data gathering to help material balance calculations. In table 4.1 the durations of all the analyzed tests are presented. Three of these are short PBUs of only ca one day, while six have lasted three days or more. From June to October 2014 an extended PBU was performed.

Table 4-1 Durations of the analyzed pressure build-up tests

PBU	Date	Shut-in (days)
1	13 Feb - 16 Feb 2013	3
2	23 Mar - 2 Apr 2013	9
3	16 Jul - 17 Jul 2013	1
4	6 Sep - 16 Sep 2013	10
5	28 Nov - 15 Dec 2013	17
6	31 Jan - 1 Feb 2014	1
7	25 Feb - 26 Feb 2014	1
8	9 Apr - 12 Apr 2014	3
9	7 Jun – 6 Oct 2014	117

For each test the analysis will be run allowing obtaining parameters specific for the best model match. Values of permeability, permeability thickness, skin, turbulence factor and the average reservoir pressure will be calculated for each case. The change of the parameters with time will be discussed.

Figure 4.1 serves as a starting point for the analysis, presenting recorded pressure response throughout the time of consideration, along with the values of preceding production rates for each case. To analyze and create the best model match for each PBU, relevant periods have been extracted and considered. The analysis will follow the following steps:

The analysis workflow:

- Data for the specific test is extracted from the history production
- The derivative of the pressure response is generated – a diagnostic plot together with a semi-logarithmic plot is created
- The model is matched and improved by means of non-linear regression
- The value of the average reservoir pressure (p*) is obtained from the pressure response in a semi-logarithmic plot from IARF regression line
- The results of each match are summarized in a table

Since the results are mainly graphic outputs from the Saphir software, the author decided to present the analysis of PBU-1, PBU-2 and PBU-9 in the main body of the report, while the results from the other tests may be observed in appendix A.

The choice has been made based on the following:

- Test number one delivers information on initial reservoir parameters, in particular, initial reservoir pressure;
- The pressure response from PBU-1 and PBU-2 will be compared and discussed
- Test number nine is an extended pressure build-up test. The obtained results are considered to be the most reliable. Also, this is the only test in which the boundaries' response is clearly seen on the plot. The distance to these boundaries was estimated and further considerations were presented.

Additionally, the quantitative summary of the results from all the tests will be presented in the form of a summary table. Chapter 4 introduces a quantitative analysis of the pressure build-up tests. Further discussions on data will be conducted in Chapter 5.

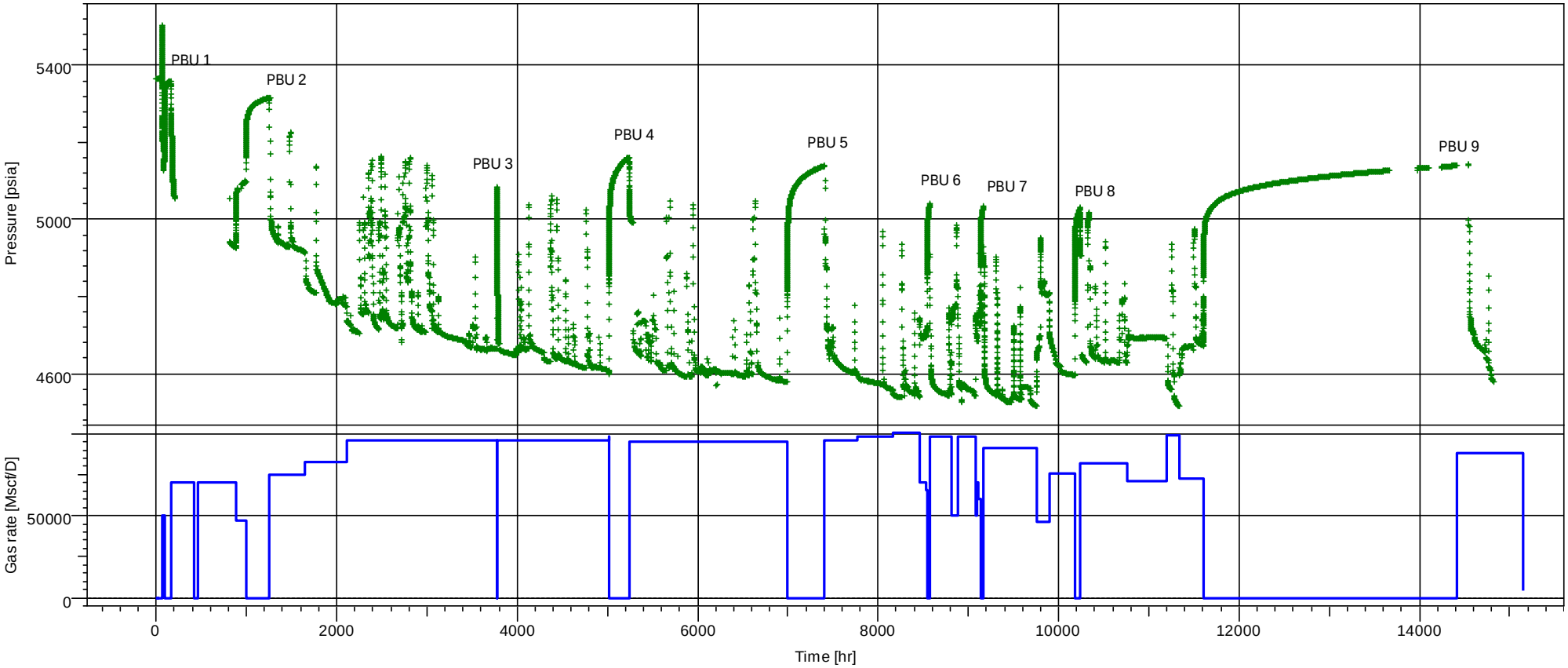

Figure 4-1: Rates and pressures history plot

.

4.2 The Analysis

PBU-1

Matched using a horizontal well model in a homogeneous reservoir of infinite extent

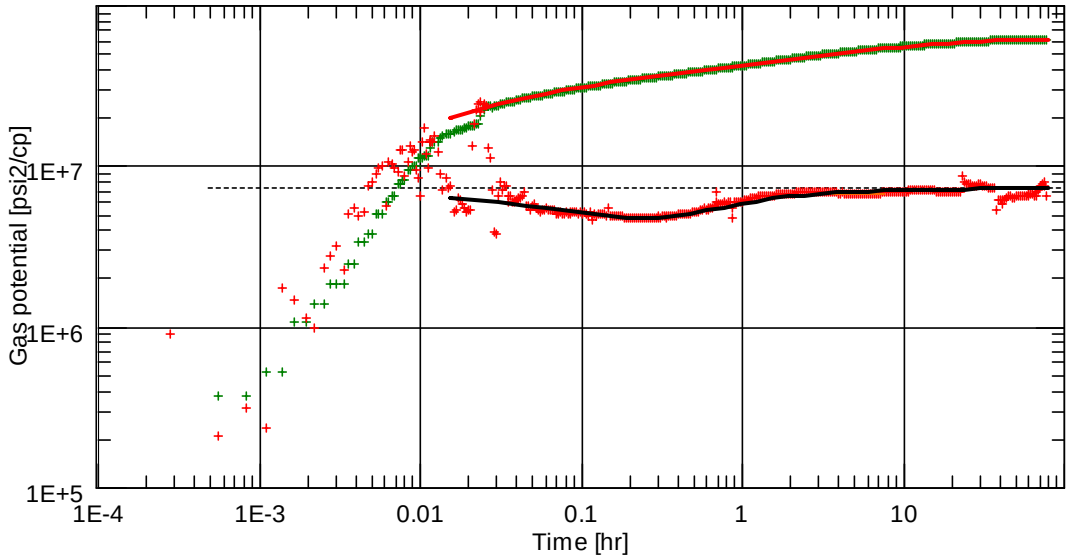

Figure 4-2: Log-log diagnostic plot for PBU-1

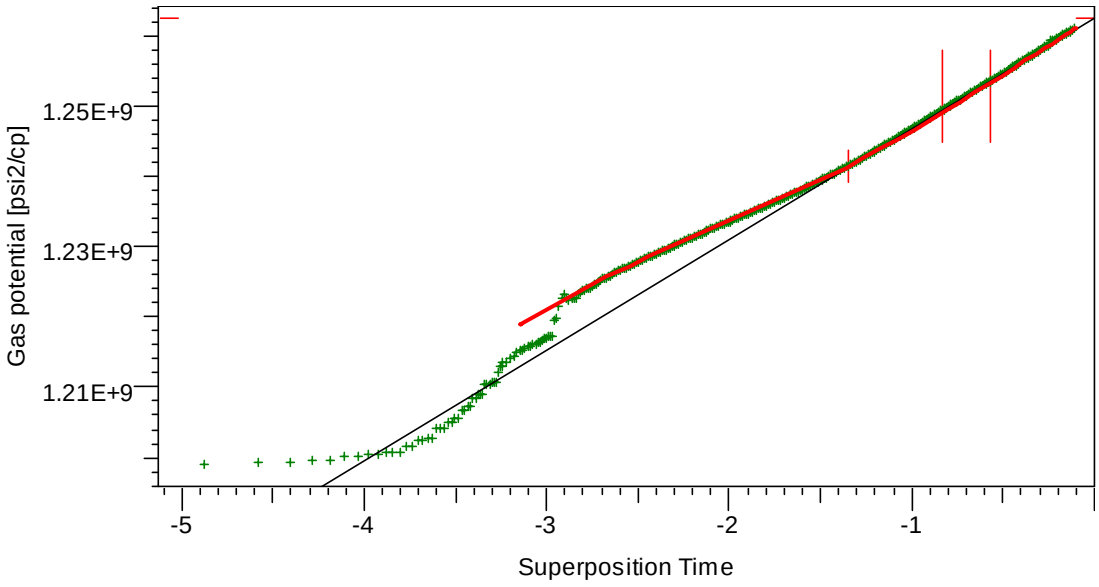

Figure 4-3: Semi-log plot for PBU-1

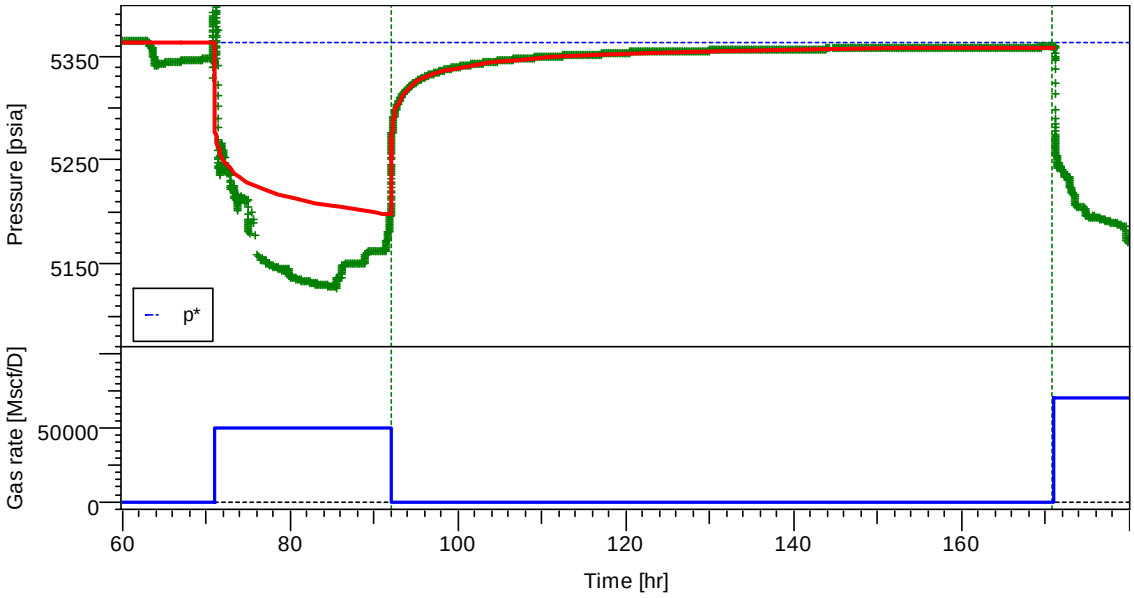

Figure 4-4: History plot for PBU-1

PBU-1 is the first from the series of the conducted tests. The model was matched using a horizontal well model in a homogeneous reservoir of infinite extent. The match-specific results can be observed in table 4-2.

Table 4-2: Model match parameters for PBU-1

Parameter	Symbol	Value	Unit
permeability thickness	kh	3250	md.ft
permeability	k	35.7	md
mechanical skin	S_0	-2.71	
total skin	S_{tot}	-4.06	
turbulence	dS/dQ	0	$[Mscf/D]^{-1}$
average pressure	p*	5362.52	psia

The log-log diagnostic plot, figure 4-2 expresses the typical response for the horizontal well. The analysis of its shape delivered the values of the initial reservoir parameters, based on well A-1 H. In the model, the skin value is not rate-dependent, thus turbulence is neglected. Skin is negative, which indicates fair productivity from the wellbore. The average reservoir pressure, which was determined by means of regression on the semi-log plot has a value of 5362.52 psia. This is the first pressure point to be used in material balance calculations for p/z method.

PBU-2

Matched using a horizontal well model in a homogeneous reservoir with parallel faults boundary

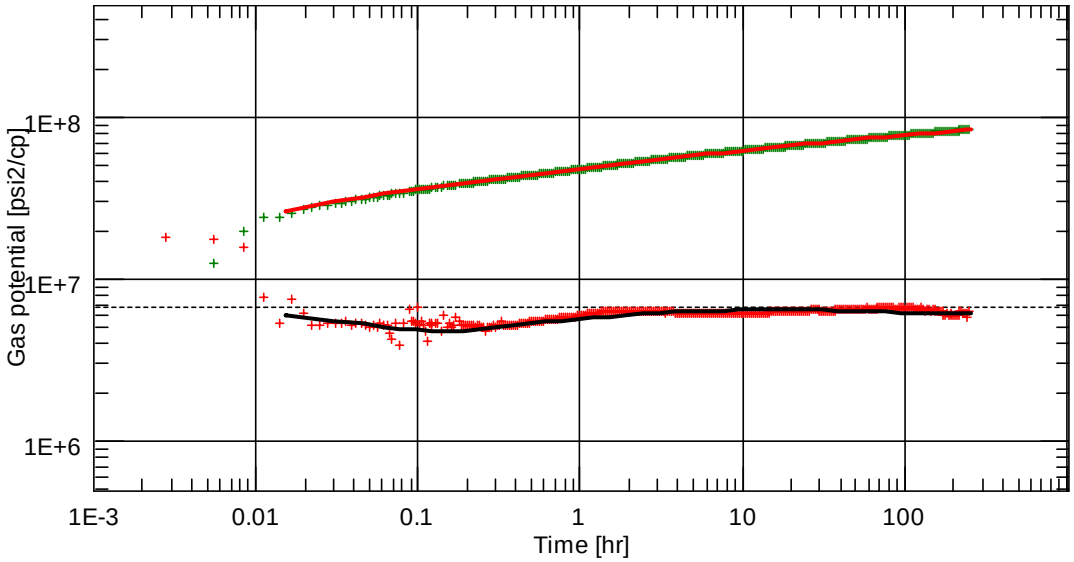

Figure 4-5: Log-log diagnostic plot for PBU-2

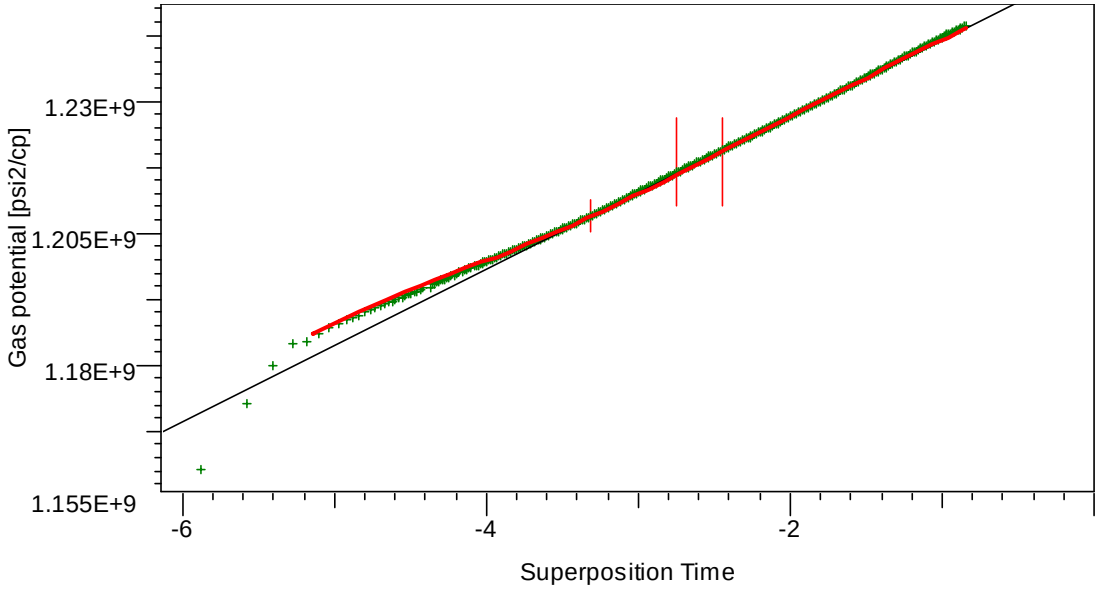

Figure 4-6: Semi-log plot for PBU-2

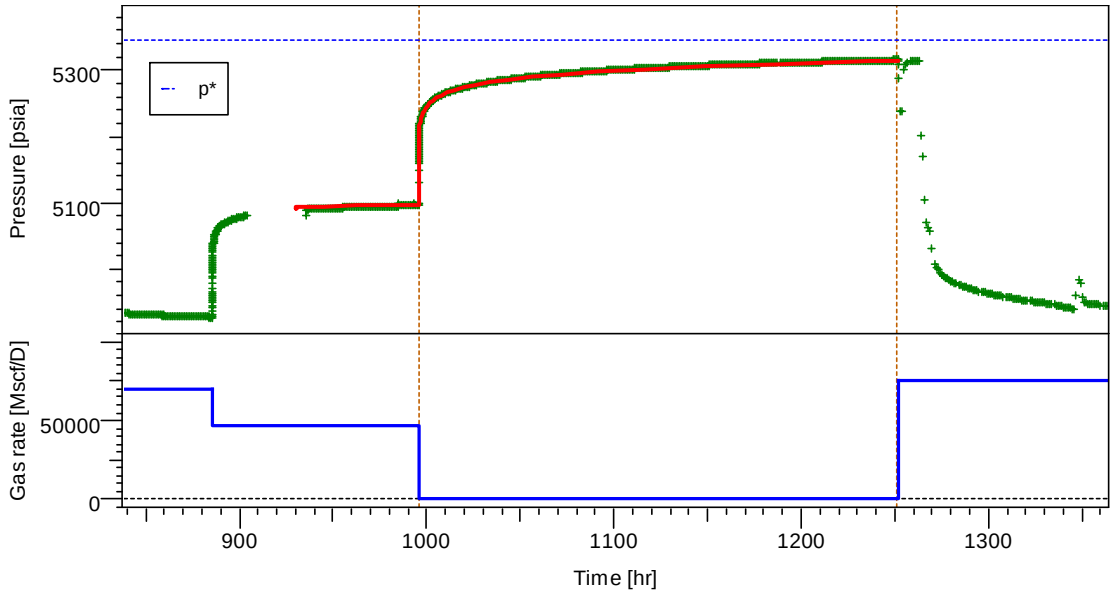

Figure 4-7: History plot for PBU-2

PBU-2 is the second of the conducted tests. The test lasted long enough for the model to be sensitive to boundaries influence. The match was obtained using a horizontal well model with parallel faults boundary. The match-specific results are summarized in table 4-3.

Table 4-3: Model match parameters for PBU-2

Parameter	Symbol	Value	Unit
permeability thickness	kh	3370	md.ft
permeability	k	37	md
mechanical skin	S_0	-3.35	
total skin	S_{tot}	-3.37	
turbulence	dS/dQ	2.6E-5	$[Mscf/D]^{-1}$
average pressure	p*	5343.46	psia
boundary 1	+y	3750	ft
boundary 2	-y	9000	ft

The pressure response from PBU-2 is consistent to PBU-1. The log-log analysis shows good repeatability indicating no large changes in well behavior, figure 4-8. Prior to PBU-2 the well was choked back to a rate of 47 MMscf/D. The change has been analyzed to derive the turbulence factor of 0.000026 $[Mscf/D]^{-1}$

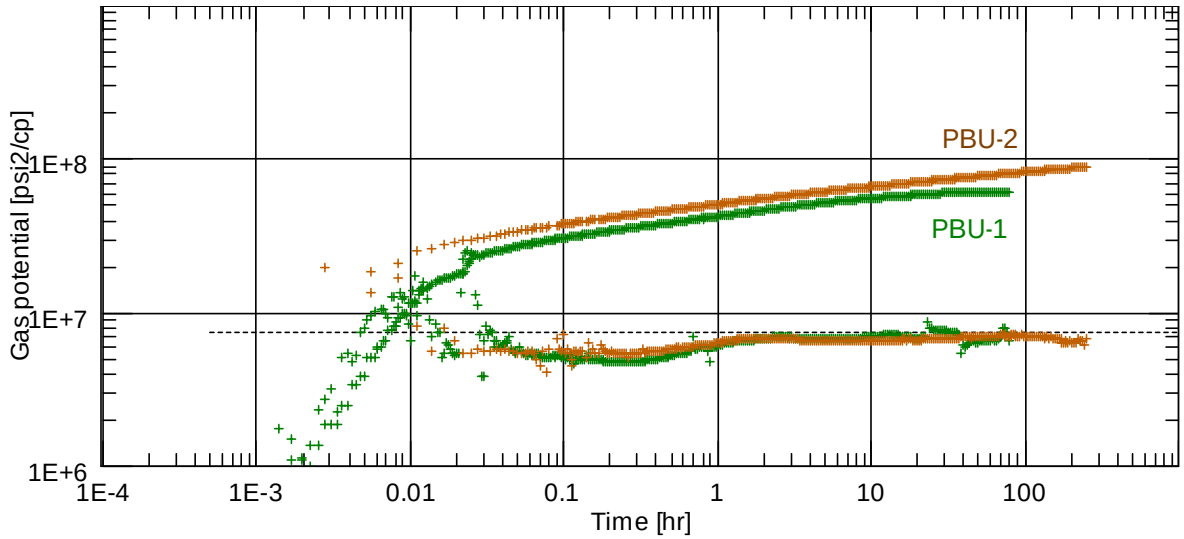

Figure 4-8: Comparison of log-log plots for PBU-1 and PBU-2

The analysis and match-specific parameters for tests PBU-3 to PBU-8 are enclosed in appendix A, along with short comments. For longer tests the shape of the pressure response is matched using horizontal well models in homogeneous reservoir bounded by two parallel faults. These are attempts to estimate and obtain the distances to the pinch-out and possible water aquifer, as indicated by seismic in figure 2-3. The responses, however, do not yet clearly indicate the deflection of the derivative as none of the tests was long enough to reach the boundaries.

The Extended PBU Analysis – PBU-9

The main reason to run the extended pressure build-up test in well A-1 H was to determine whether the aquifer response can be seen and to obtain more accurate pressure values for material balance calculations. Shut-in pressure data from almost 120 days has been used in the analysis. The main difference between this PBU and the earlier PBUs is that the clear turn-up of the derivative shows up after ca 600 hours (figure 4-9); this is the boundaries' response. Table 4-4 summarizes obtained values of the dynamic parameters. The test will be further discussed in Chapter 5.

PBU-9

Matched using a horizontal well model in a homogeneous reservoir with parallel faults boundary

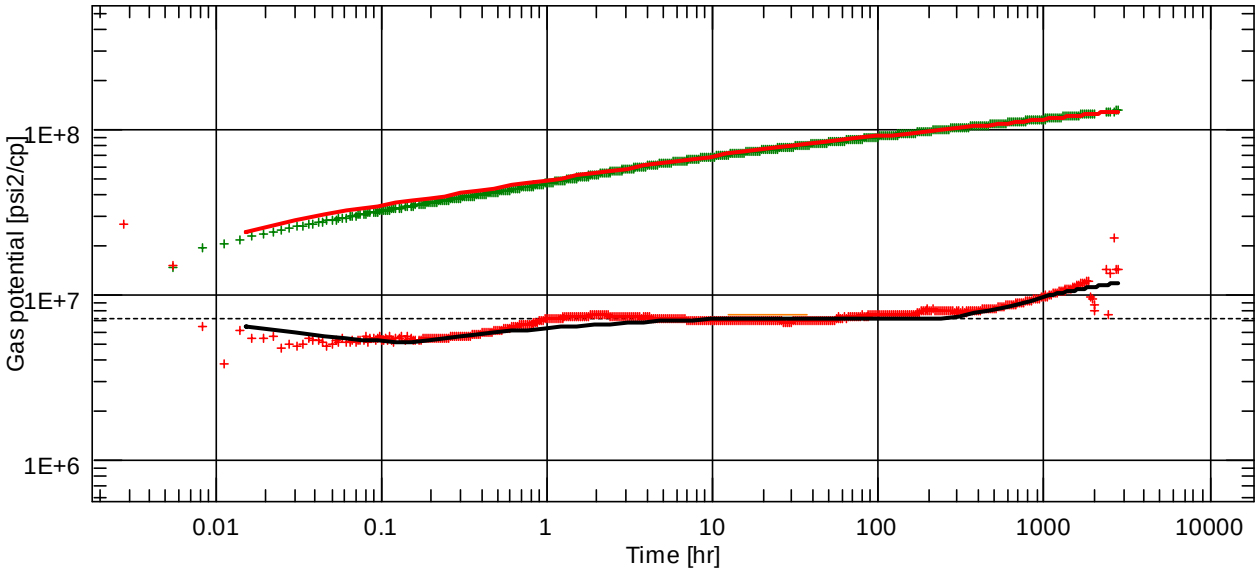

Figure 4-9: Log-log diagnostic plot for PBU-9

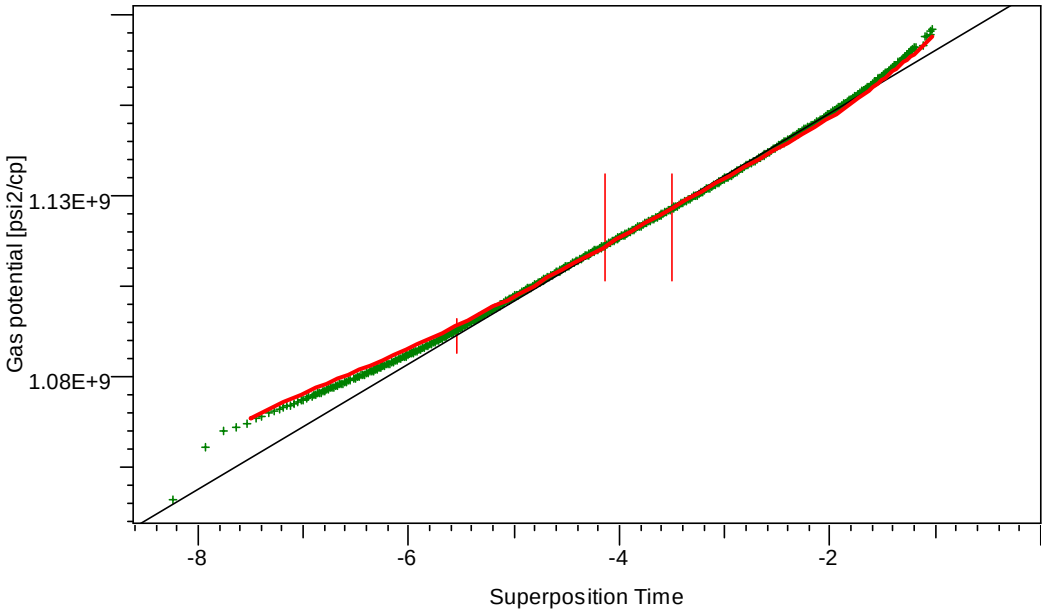

Figure 4-10: Semi-log plot for PBU-9

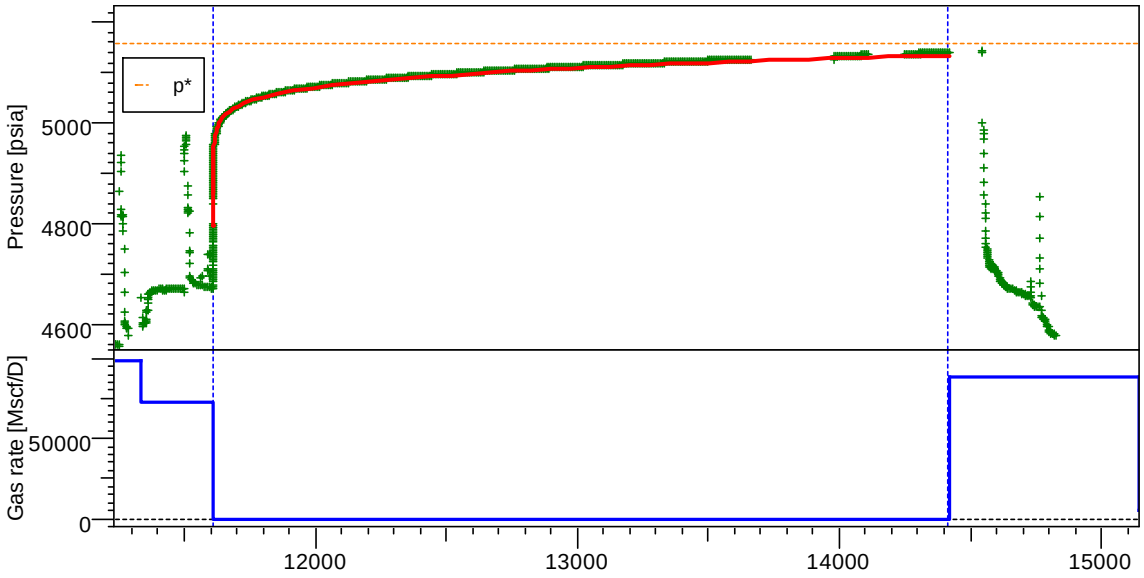

Figure 4-11: History plot for PBU-9

Table 4-4: Model match parameters for PBU-9

Parameter	Symbol	Value	Unit
permeability thickness	kh	3620	md.ft
permeability	k	39.8	md
mechanical skin	S_0	-4.9	
total skin	S_{tot}	-3.75	
turbulence	dS/dQ	4.39E-5	$[Mscf/D]^{-1}$
average pressure	p*	5155.94	psia
boundary 1	+y	4800	ft
boundary 2	-y	30000	ft

Chapter 5 Results and Discussions

In this chapter the summary of the results obtained from the PBUs analysis will be presented and discussed.

Figure 5-1 shows an overlay of the derivative plots from the main PBUs longer than 1 day. There is generally good agreement between all the tests, indicating that the estimates for permeability thickness product kh are quite reliable.

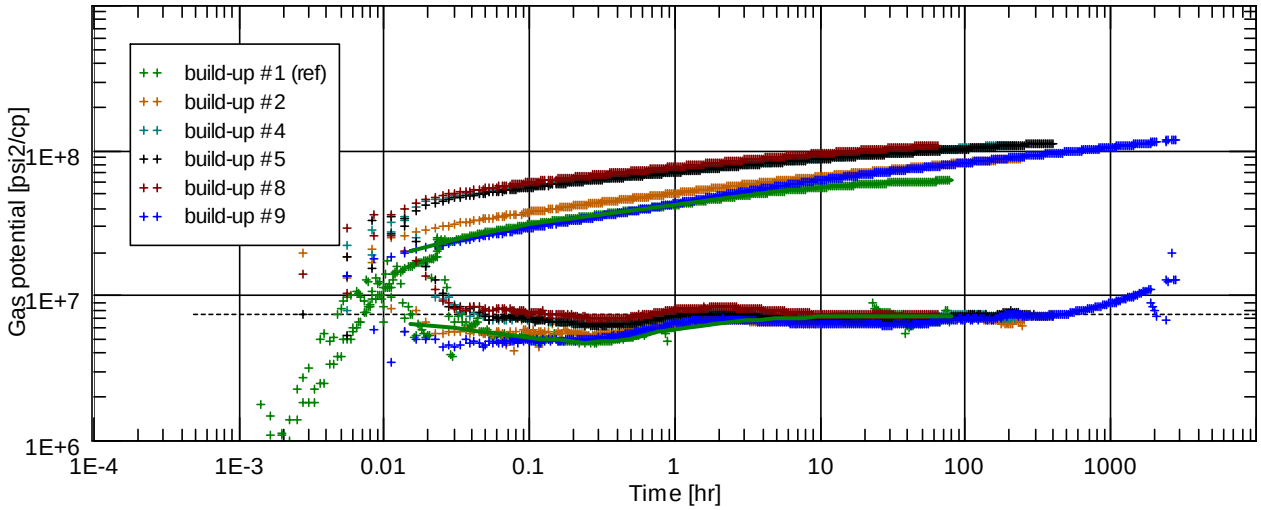

Figure 5-1: Derivative overlay from main PBUs

Table 5-1 has been put together to summarize obtained values of permeability, permeability thickness and skin for all the PBUs.

Table 5-1: Summary of the dynamic parameters values

Parameter	PBU-1	PBU-2	PBU-3	PBU-4	PBU-5	PBU-6	PBU-7	PBU-8	PBU-9
Permeability thickness, md.ft	3250	3370	3070	3350	3350	3320	3320	3060	3620
Permeability, md	35.7	37	33.7	36.8	36.8	36.5	36.5	33.7	39.8
Mechanical skin	-2.71	-3.35	-1.7	-2.2	-1.8	-2.25	-3.4	-1.56	-4.9
Total skin	-4.06	-3.37	-2.4	-1.87	-1.89	-2.24	-2.79	-1.89	-3.75

- The obtained values of permeability thickness, kh, oscillate around 3300 md.ft in most of the tests. The greatest value of 3620 md.ft is observed in case of the extended PBU.
- In each test, the value of skin factor is negative. That indicates good well productivity.
- Parameters from test number 3 may be encumbered with errors because the test lasted only couple of hours and the IARF straight line on the pressure response was not reached.
- The parameters obtained from an extended PBU should be treated as the most reliable and best illustrating the behavior of the reservoir, as the infinite acting radial flow regime is well developed and boundaries are reached.

Additionally, the average reservoir pressures p* obtained from semi-log plots for each test are tabulated in table 5-2.

Table 5-2: Extrapolated values of reservoir pressure:

PBU	Average reservoir pressure p*, psia
1	5362.52
2	5343.46
3	5310.14
4	5256.24
5	5218.06
6	5206.97
7	5198.64
8	5182.86
9	5155.94

The values of the average reservoir pressure decrease with time. The initial reservoir pressure is at the level of 5362.52, while the extrapolated pressure after the PBU-9 is 5155.94. There seems to be a good agreement between the obtained values, however, this can be only confirmed by material balance calculations. Also, further study in that subject would allow indicating the dominating drive mechanism for the Snadd reservoir.

Test number nine was an extended pressure build-up test. A clear turn-up of the derivative is observed after ca 600 hours, which indicates the existence of the boundaries. The distances to these boundaries were estimated, approximately 4800 ft (1463 m) and 30000 ft (~9140 m). The

closer boundary might be interpreted to be the aquifer response. It lies between the minimum (680 m) and maximum (2200 m) distances to the aquifer, as shown in figure 2-3.

None of the tests detected the third boundary of the reservoir, which goes in line with the current knowledge of the structure geometry (narrow, long structure). Therefore it might be possible that the Snadd North and Snadd South structures are in communication.

Data obtained from pressure build-up tests should not be interpreted with no support of geological or geophysical information, as in the simulators the same model match might be obtained for altering values of certain parameters.

Chapter 6 Conclusions

The intention of this study was to obtain approximate values of dynamic reservoir parameters of the Snadd field, through the analysis of well test data from well A-1 H. With the use of Saphir software nine pressure build-up tests were analyzed. Short tests were matched using a horizontal well model in a homogeneous reservoir of infinite extent and longer were matched assuming a parallel fault boundary.

The analysis of the data from test number one provided the values of the initial reservoir parameters.

There is a good repeatability between the main tests, which indicates reliable estimates of permeability thickness product.

Throughout all the test periods skin values remained negative; obtained parameters indicate good wellbore productivity.

The pressure response from the last of the tests, test number nine, clearly indicated the presence of the boundaries. The considerations of the possible aquifer were discussed and the matched distance of 1463 m stayed within the distances estimated by the geological and seismic data.

None of the tests detected the third boundary, which confirms the information about the long and thin field structure. The Snadd North structure might be in communication Snadd South structure.

References

1. BP, Well 65075-6 S and well 65075-6 ST2 Snadd North discovery report. Internal document. 2010.
2. BP, Snadd Well 65075-A-1 H Test Production Report 1. Internal document. 2013.
3. BP, Snadd Well 65075-A-1 H Test Production Report 3. Internal document. 2014.
4. BP, Snadd North Producer. Statement of Requirement part 2. Internal document. 2011.
5. Muskat, M., Use of Data on the Build-up of Bottom-hole Pressures. Society of Petroleum Engineers, SPE-937044, 1936.
6. Miller, C.C., A.B. Dyes, and C.A. Hutchinson Jr, The estimation of permeability and reservoir pressure from bottomhole pressure build-up characteristics. 1950.
7. Horner, D.R., Pressure Build-Up in Wells, in 3rd World Petroleum Congress, 28 May-6 June. 1951, World Petroleum Congress: Hague, the Netherlands.
8. Perrine, R.L., Analysis of Pressure-buildup Curves. 1956, American Petroleum Institute.
9. Ramey Jr., H.J., Short-Time Well Test Data Interpretation in the Presence of Skin Effect and Wellbore Storage, SPE-2336. Journal of Petroleum Engineering, January 1970: p. 97-104.
10. [cited 2015 20/06]; Available from: http://petrowiki.org/Type_curves#Dimensionless_variables.
11. Earlougher Jr., R.C. and K.M. Kersch, Analysis of Short-Time Transient Test Data by Type-Curve Matching, SPE-004488. Journal of Petroleum Technology, July 1974: p. 793-800.
12. Gringarten, A.C., et al., A comparison between different skin and wellbore storage type-curves for early-time transient analysis. 1979, SPE-008205.
13. Bourdet, D., et al., A new set of type curves simplifies well test analysis. World Oil, May 1983.
14. BP, Skarv-Idun ISD. Internal document. 2010.
15. BP, Application for Test Production from the Snadd North well 6507/5-A-1 H. Internal document. 2010.
16. BP, Snadd Model History Match. Internal document. 2015.
17. PERA, Snadd Fluid Study. Internal document. 2012.
18. BP, Skarv Development Project. Statement of Requirement part 1. Internal document. 2011.
19. Ahmed, T., Reservoir Engineering Handbook. 2010.
20. Bourdet, D., Well Test Analysis: The Use of Advanced Interpretation Models. 2002.
21. Houze, O., D. Viturat, and O.S. Fjaere, Dynamic Data Analysis. 2012, KAPPA.
22. Zolotukhin, A.B. and J.-R. Ursin, Introduction to petroleum reservoir engineering. 1997.
23. Earlougher Jr., R.C., Advances in well test analysis. SPE Monograph Series, Vol. 5. 1977: Society of Petroleum Engineers of AIME.
24. Schlumberger, Introduction to Well Testing. 1998.

Nomenclature

p_D	dimensionless pressure
t_D	dimensionless time
p	pressure
t_p	production time prior to shut-in
Δt	wellbore shut-in time
k	permeability
kh	permeability thickness product
h	formation thickness
q	flow rate
μ	viscosity of fluid
B	Formation volume factor
m	semi-log slope line
s	skin factor
s_0	mechanical skin
s_G	geometrical skin
p_{1h}	pressure after 1 hour
p_{wf}	wellbore pressure
ϕ	porosity
c_t	total compressibility
r_w	wellbore radius
C	wellbore storage
Q	flow rate
A	cross-section area
L	length

Appendix A – The results of the Simulations

i. PBU-3

Matched using a horizontal well model in a homogeneous reservoir of infinite extent

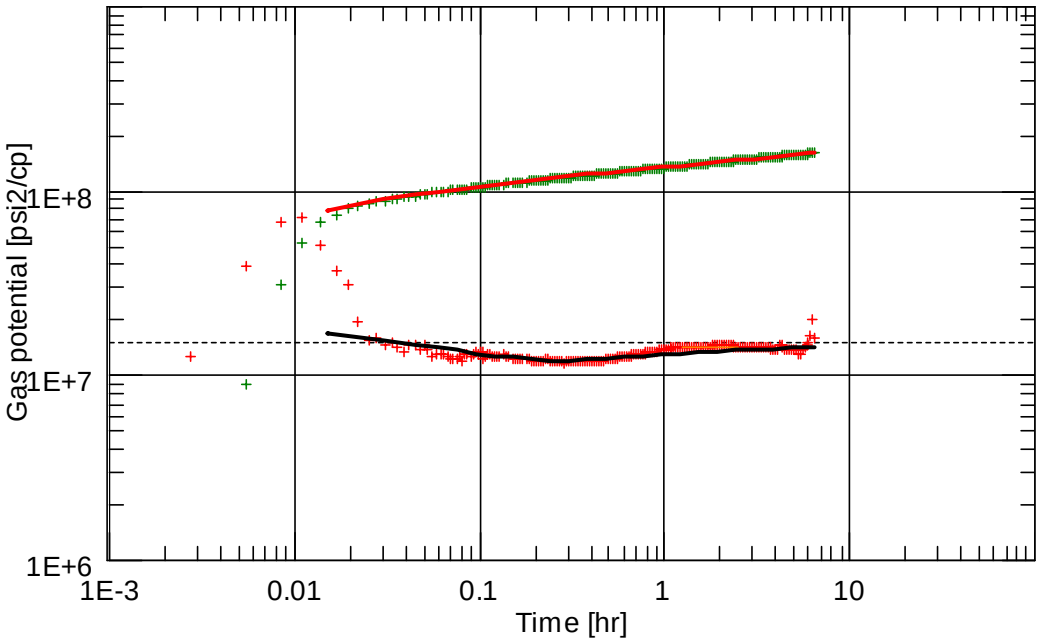

Figure 0-1: Log-log diagnostic plot for PBU-3

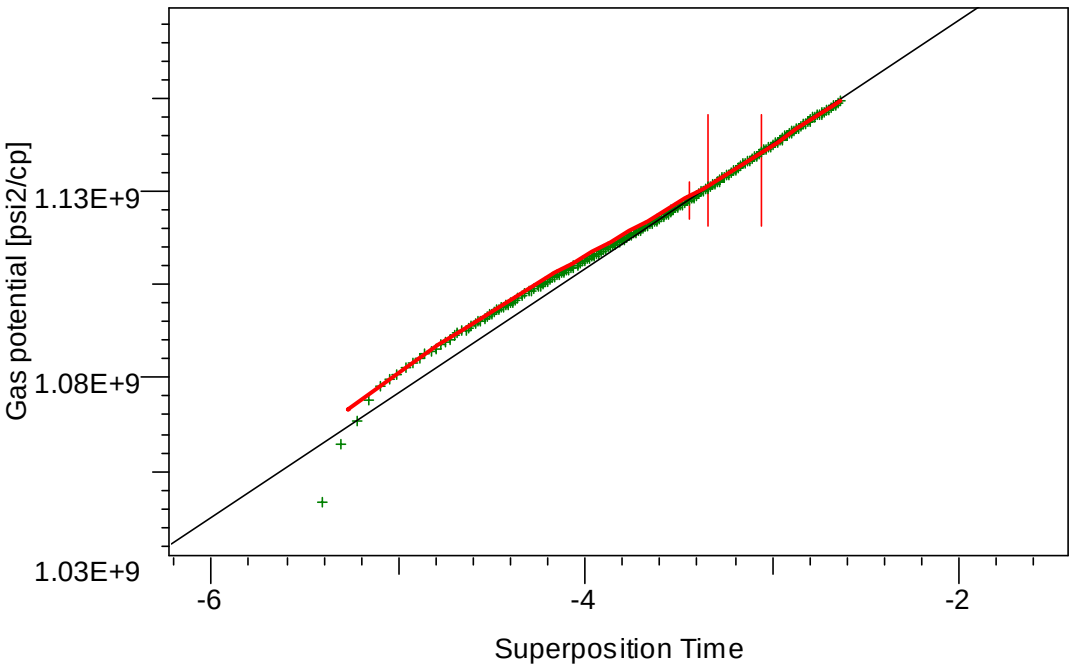

Figure 0-2: Semi-log plot for PBU-3

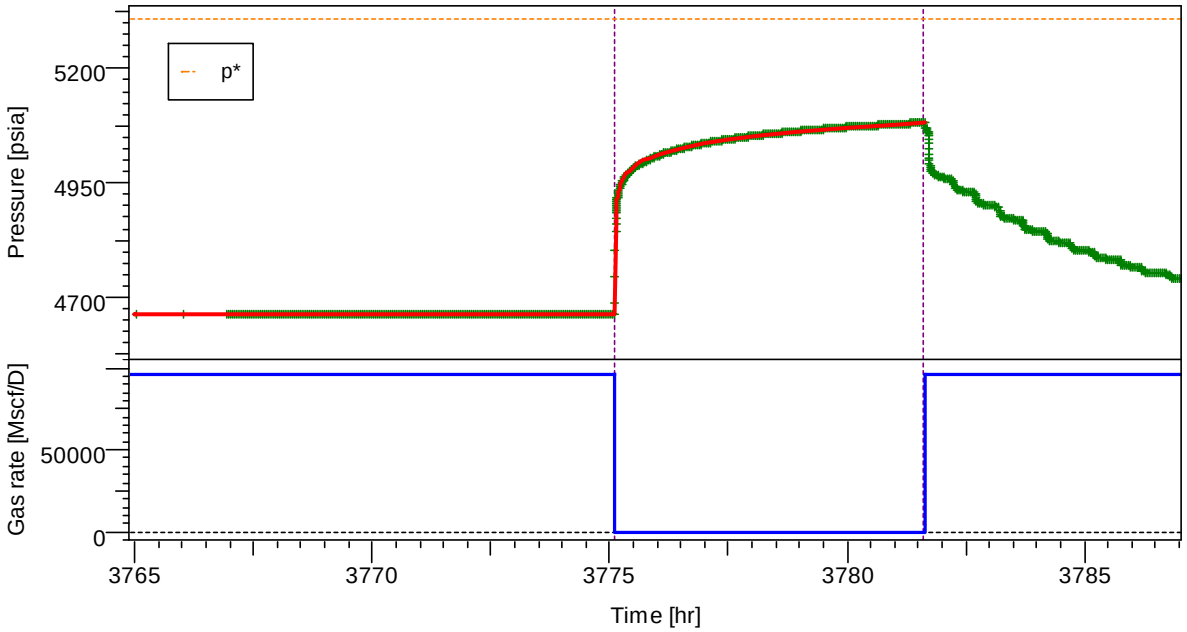

Figure 0-3: History plot for PBU-3

The third test in the sequence, PBU-3, was the shortest of all the tests. The shut-in period lasted only for ca 7 hours. The match was obtained using a horizontal well model in homogeneous reservoir of infinite extent. Because the IARF straight line was not reached in the pressure response, the results might be encumbered with errors. The match specific results are presented in table 0-2.

Table 0-1: Model match parameters for PBU-3

Parameter	Symbol	Value	Unit
permeability thickness	kh	3070	md.ft
permeability	k	33.7	md
mechanical skin	S_0	-1.7	
total skin	S_{tot}	-2.4	
turbulence	dS/dQ	0	$[Mscf/D]^{-1}$
average pressure	p*	5310.14	psia

ii. PBU-4

Matched using a horizontal well model in a homogeneous reservoir with parallel faults boundary

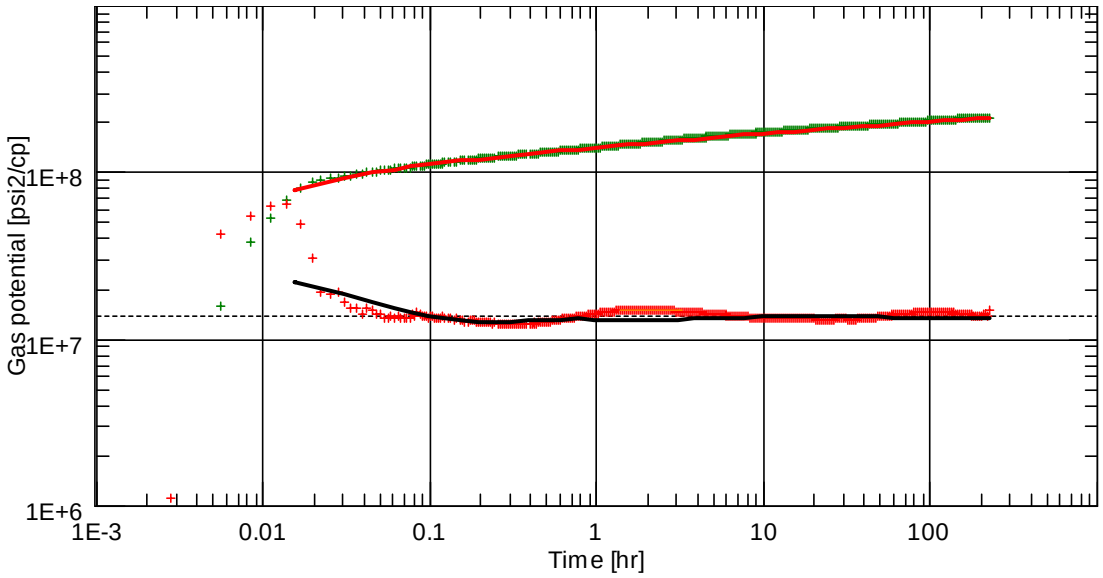

Figure 0-4: Log-log diagnostic plot for PBU-4

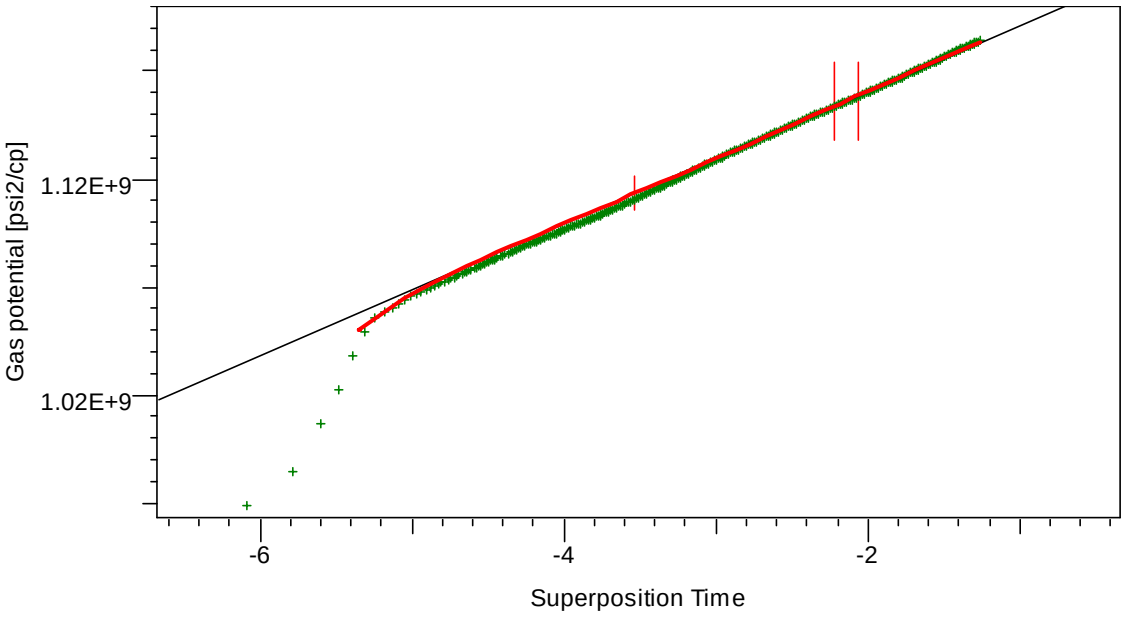

Figure 0-5: Semi-log plot for PBU-4

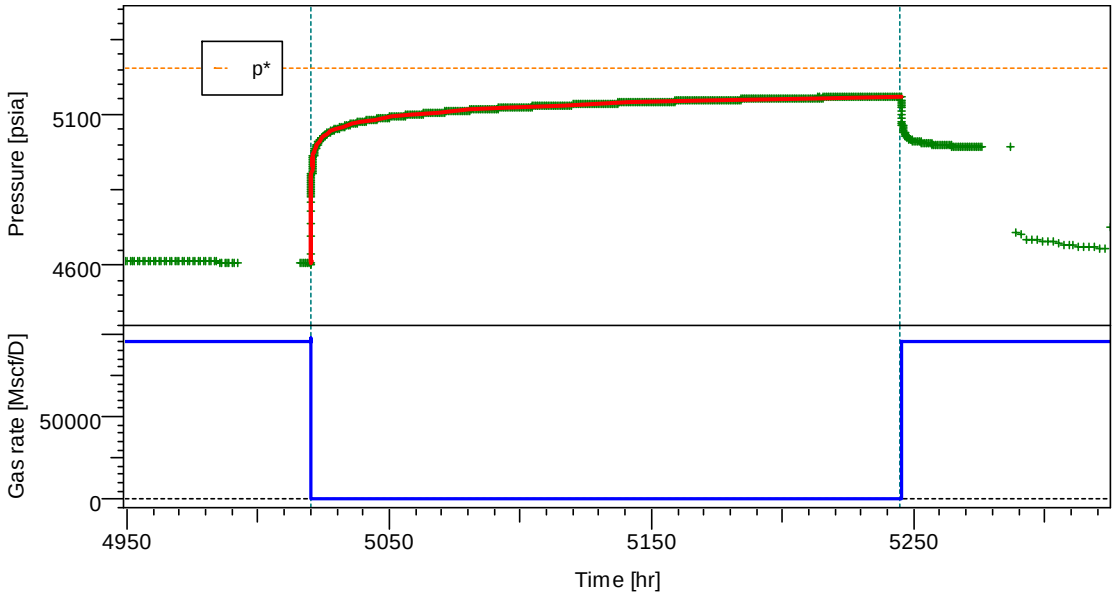

Figure 0-6: History plot for PBU-4

The fourth test, PBU-4 lasted for ca 10 days. In the pressure derivative response, a “hump” may be observed in the first few hours of the build-up response. This might be one of the implications of the unusual well geometry (figure 2-2). The shape of the match curve was influenced by boundaries; to obtain a match a model of a well in homogeneous reservoir with parallel faults boundary was used. The match data is put together in table 0-3.

Table 0-2: Model match parameters for PBU-4

Parameter	Symbol	Value	Unit
permeability thickness	kh	3350	md.ft
permeability	k	36.8	md
mechanical skin	S_0	-2.2	
total skin	S_{tot}	-1.87	
turbulence	dS/dQ	7.66E-6	$[Mscf/D]^{-1}$
average pressure	p*	5256.24	psia
boundary 1	+y	3900	ft
boundary 2	-y	9000	ft

iii. PBU-5

Matched using a horizontal well model in a homogeneous reservoir with parallel faults boundary

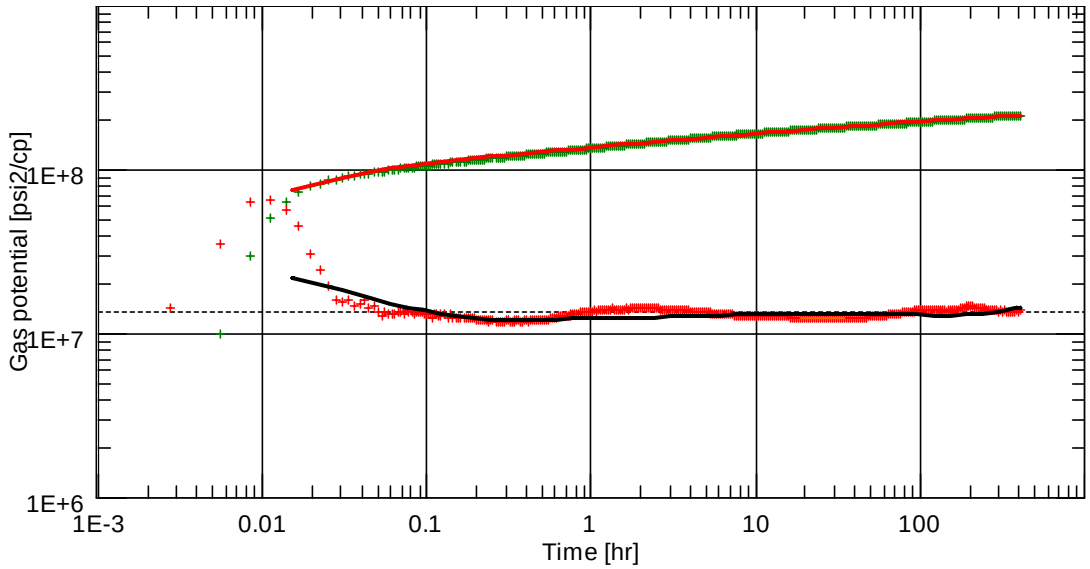

Figure 0-7: Log-log diagnostic plot for PBU-5

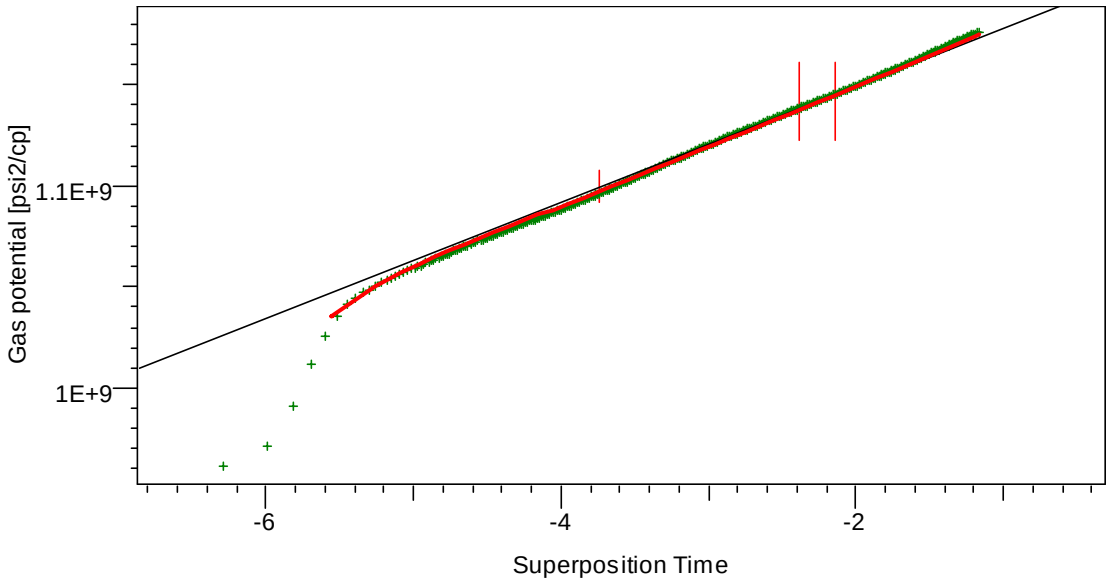

Figure 0-8: Semi-log plot for PBU-5

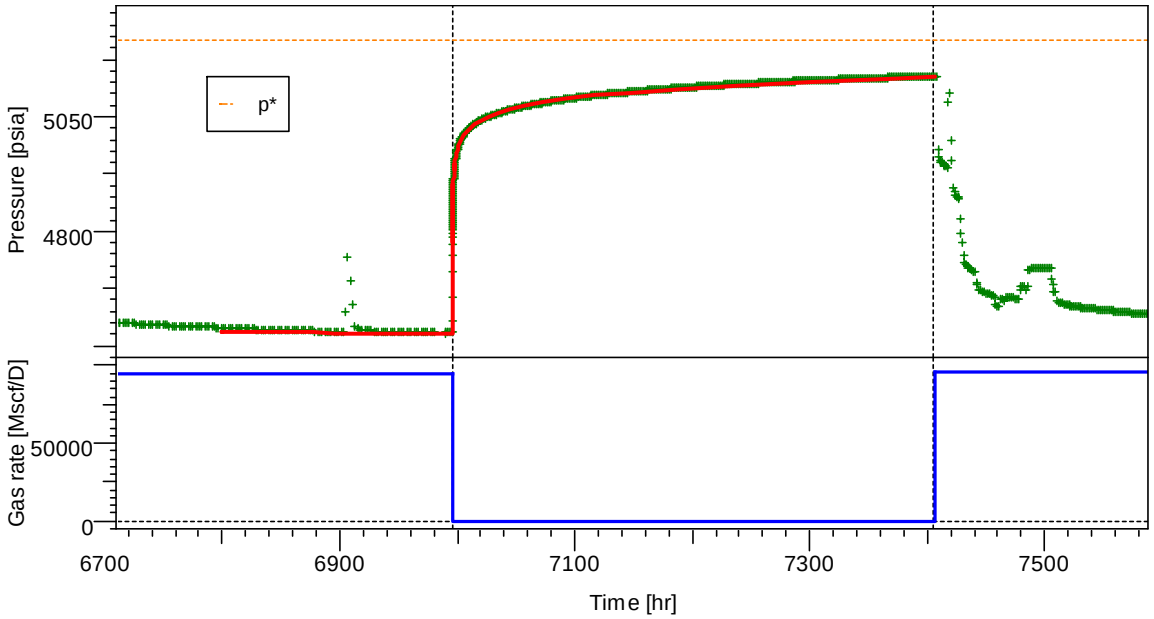

Figure 0-9: History plot for PBU-5

PBU-5 started at the end of November 2013 and lasted for a period of 17 days. The pressure response seem to go in line with what could be observed during PBU-4. Similarly, the match was obtained using a horizontal well model in homogeneous reservoir with parallel faults boundary. The results are tabulated in table 0-4.

Table 0-3: Model match parameters for PBU-5

Parameter	Symbol	Value	Unit
permeability thickness	kh	3350	md.ft
permeability	k	36.8	md
mechanical skin	S_0	-1.8	
total skin	S_{tot}	-1.89	
turbulence	dS/dQ	3E-6	$[Mscf/D]^{-1}$
average pressure	p*	5218.06	psia
boundary 1	+y	3900	ft
boundary 2	-y	10000	ft

iv. PBU-6

Matched using a horizontal well model in a homogeneous reservoir of infinite extent

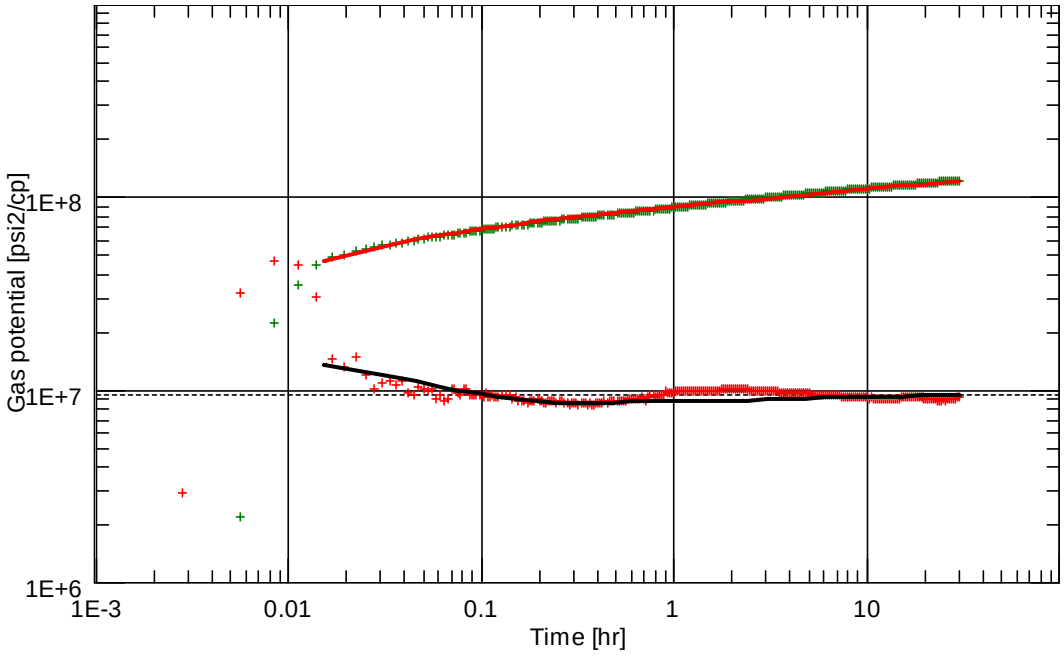

Figure 0-10: Log-log diagnostic plot for PBU-6

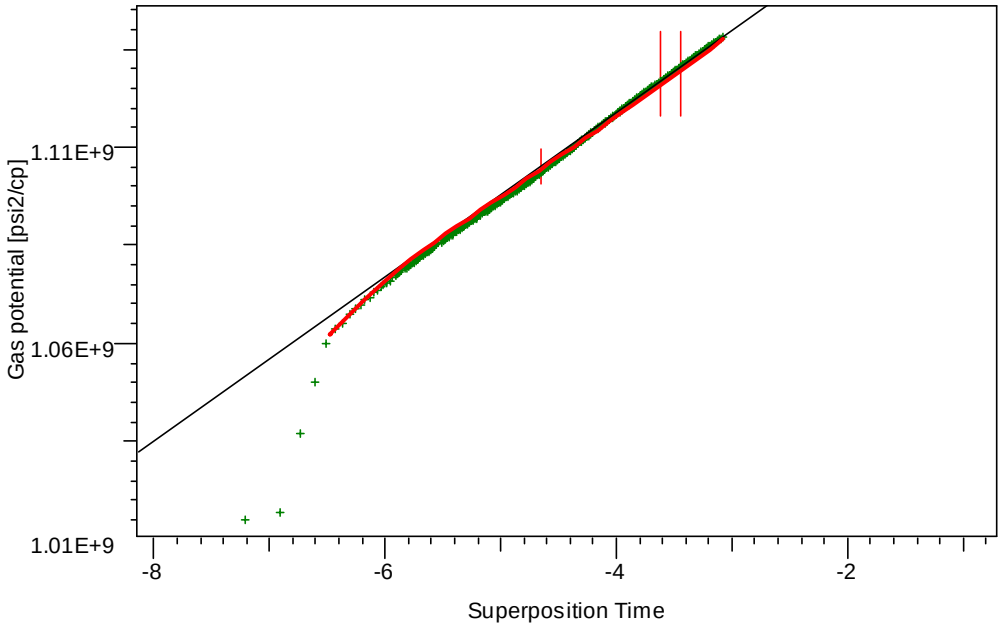

Figure 0-11: Semi-log plot for PBU-6

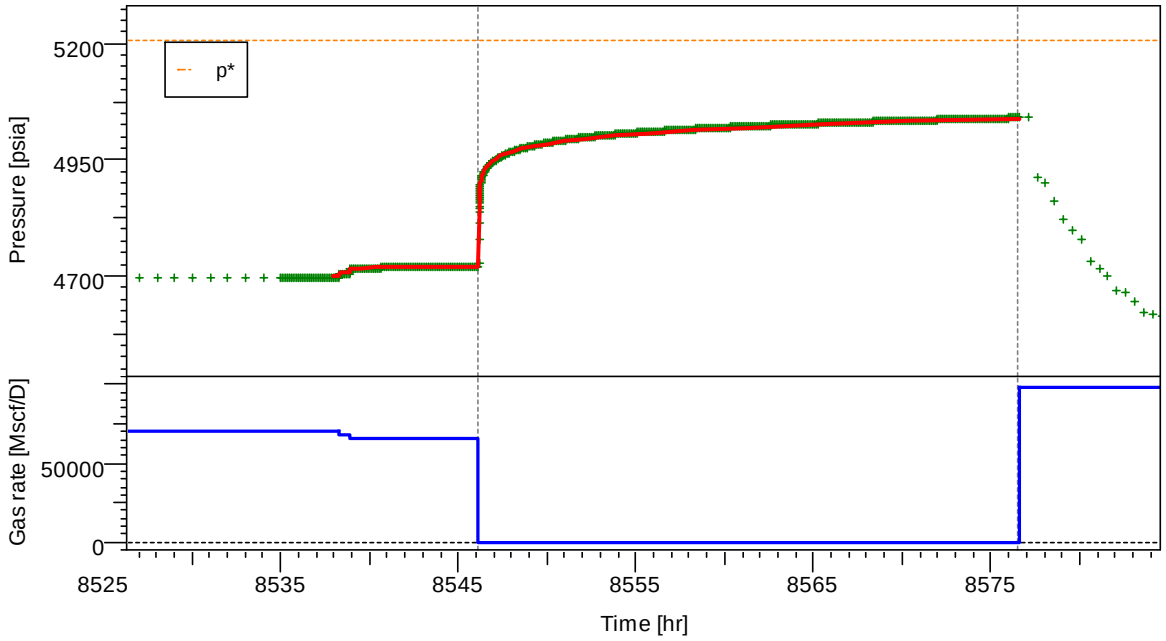

Figure 0-12: History plot for PBU-6

PBU-6 is another short test in the test sequence, but it is longer than test number 3. The match was obtained using a horizontal well model in homogeneous reservoir of infinite extent. The match-specific parameter values may be observed in table 0-5.

Table 0-4: Model match parameters for PBU-6

Parameter	Symbol	Value	Unit
permeability thickness	kh	3320	md.ft
permeability	k	36.5	md
mechanical skin	S_0	-2.25	
total skin	S_{tot}	-2.24	
turbulence	dS/dQ	5.9E-6	$[Mscf/D]^{-1}$
average pressure	p*	5206.97	psia

v. PBU-7

Matched using a horizontal well model in a homogeneous reservoir of infinite extent

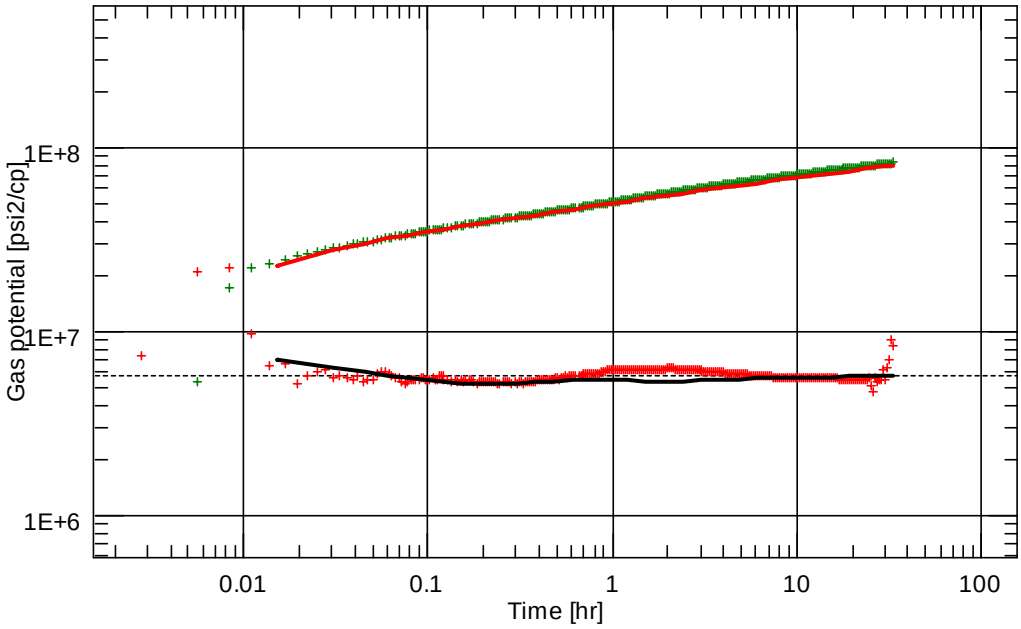

Figure 0-13: Log-log diagnostic plot for PBU-7

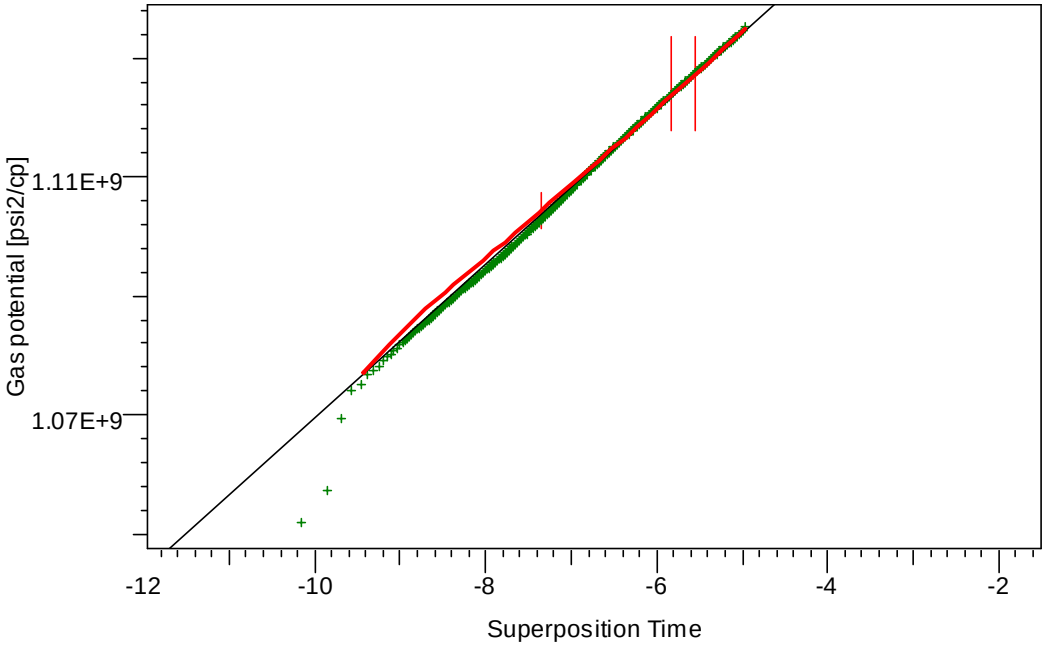

Figure 0-14: Semi-log plot for PBU-7

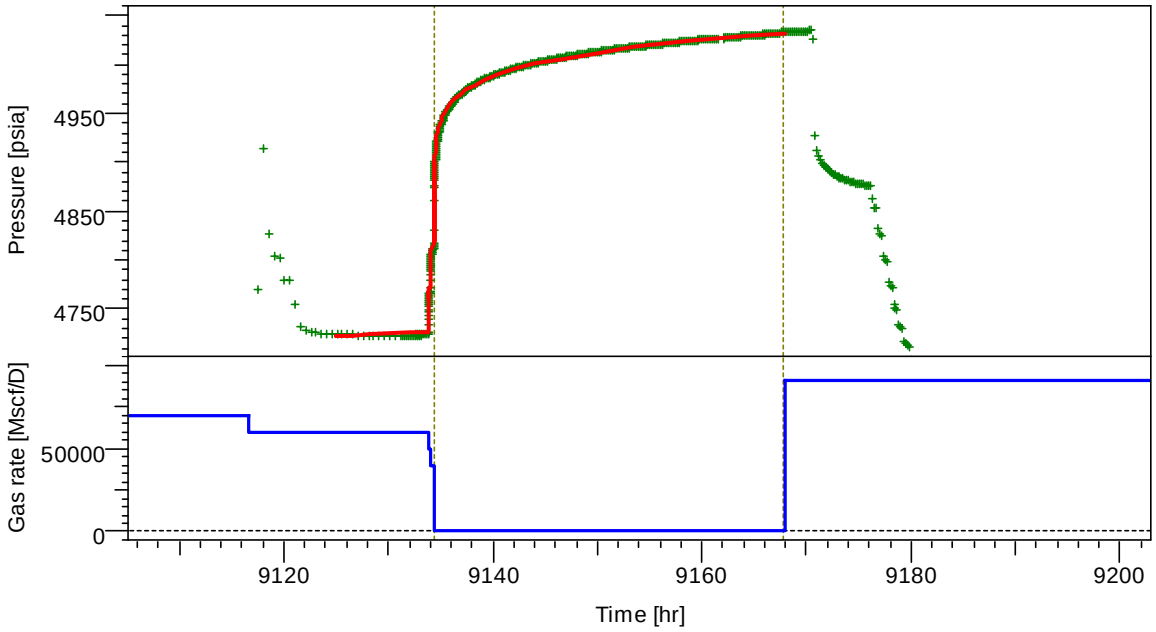

Figure 0-15: History plot for PBU-7

Similarly to PBU-6, PBU-7 is another short time test. The match was obtained using a horizontal well model in homogeneous reservoir of infinite extent. As can be observed on a semi-log response, figure 0-14, there is a slight mismatch in the early time data.

Table 0-5: Model match parameters for PBU-7

Parameter	Symbol	Value	Unit
permeability thickness	kh	3320	md.ft
permeability	k	36.5	md
mechanical skin	S_0	-3.4	
total skin	S_{tot}	-2.79	
turbulence	dS/dQ	2.95E-5	$[Mscf/D]^{-1}$
average pressure	p*	5198.64	psia

vi. PBU 8

Matched using a horizontal well model in a homogeneous reservoir of infinite extent

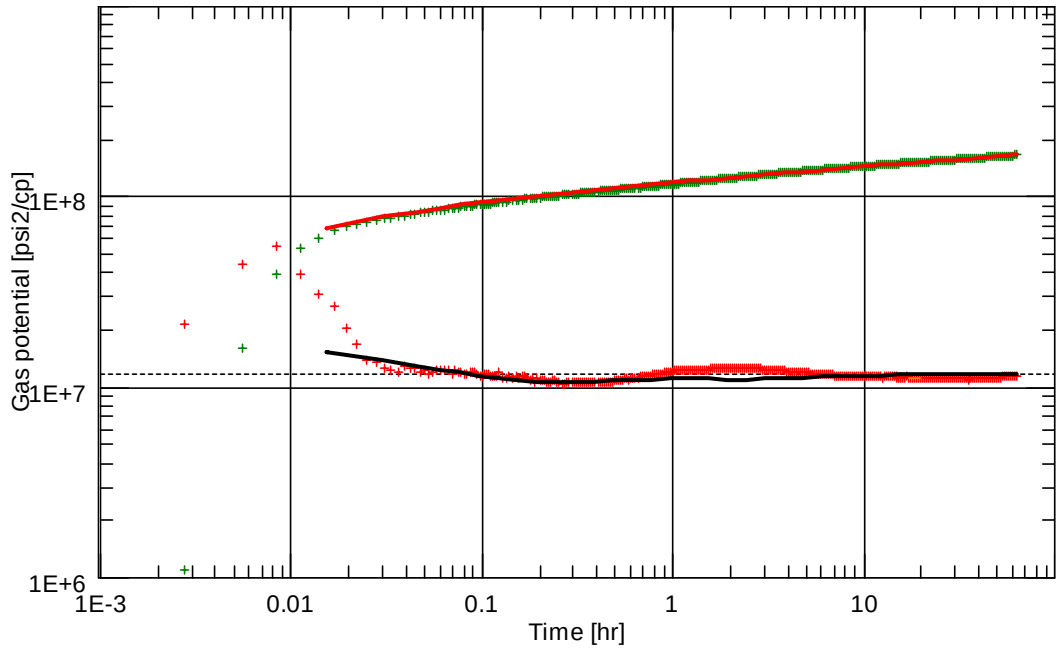

Figure 0-16: Log-log diagnostic plot for PBU-8

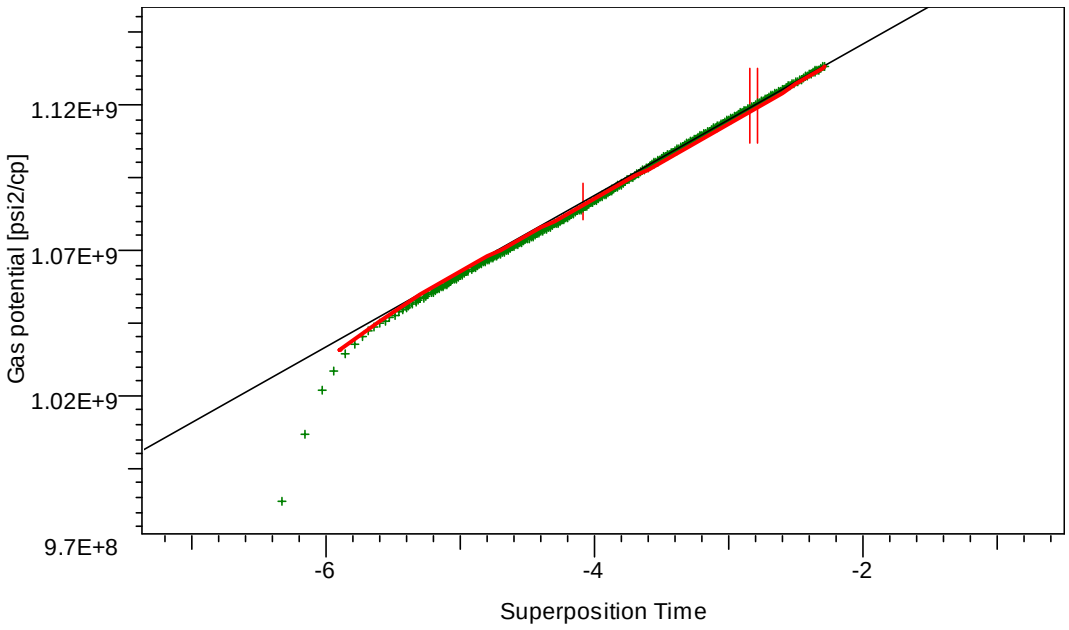

Figure 0-17: Semi-log plot for PBU-8

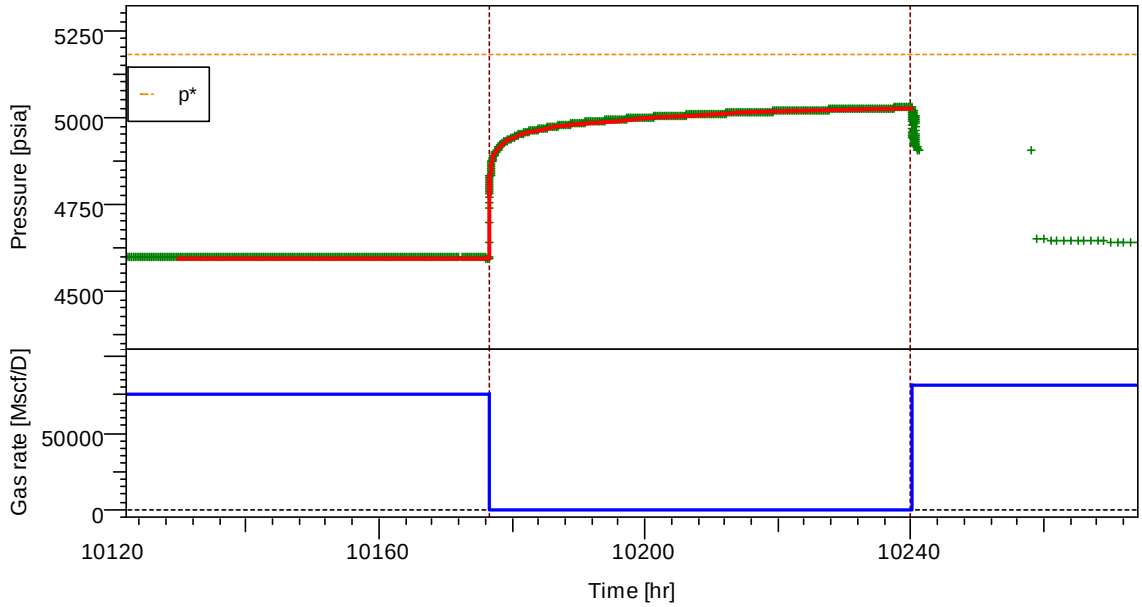

Figure 0-18: History plot for PBU-8

The model for PBU-8 was matched using a horizontal well model in homogeneous reservoir of infinite extent. The parameters for the model are presented in table 0-6.

Table 0-6: Model match parameters for PBU-8

Parameter	Symbol	Value	Unit
permeability thickness	kh	3060	md.ft
permeability	k	33.7	md
mechanical skin	S_0	-1.56	
total skin	S_{tot}	-1.89	
turbulence	dS/dQ	0	$[Mscf/D]^{-1}$
average pressure	p*	5182.86	psia